

Chalcogenide Topological Insulators

Joseph A. Haggmann

*Physical Measurement Laboratory, National Institute for Standards and Technology, Gaithersburg,
MD 20899, USA.*

Corresponding author email: joseph.haggmann@nist.gov

I. Preface

The purpose of this chapter is to introduce the reader to the chalcogenide materials systems that host the *topological insulator* phase of quantum matter. Specifically, the HgTe quantum well 2D topological insulator system and the V_2VI_3 -type bismuth- and antimony-chalcogenide 3D topological insulator systems will be described. The chapter includes a general introduction to topological insulator systems, a description of the various growth methods for the synthesis of chalcogenide topological insulator materials, a review of notable studies and discoveries along with a description of several exotic topological states that have been shown to exist or are predicted to exist in these materials, and an outlook and summary.

II. Introduction

An exotic phase of quantum matter exists in certain classes of chalcogenide materials, characterized by strong spin-orbit coupling and hosting time-reversal invariant systems, is the topological insulator (TI). Topological insulators are materials with a bulk band gap and band-crossing edge states or surface states supported by the non-trivial band topology of the TI. The topologically protected states are helical, with the electron spin locked perpendicular to the momentum, protecting against direct backscattering by non-magnetic impurities. The

chalcogenide topological insulators discussed in this chapter are of two types. The first is the 2D topological insulator system observed in type-III HgTe semiconductor quantum wells, which hosts topologically protected edge states with a quantized conductance arising from the quantum spin Hall effect, and the V_2VI_3 -type bismuth- and antimony-chalcogenide 3D topological insulators.

The existence of a phase of exotic quantum matter in systems with time-reversal symmetry was found to be rather unexpected, as prior to the discovery of symmetry-protected topological states, [1, 2] exotic quantum states were believed to arise from symmetry breaking according to the Landau paradigm. [3] Symmetry-breaking exotic quantum phenomena include superconductivity, which arises when the electromagnetic gauge symmetry associated to electron number is broken, [4] and ferromagnetism, which arises when time-reversal symmetry is broken. [5] Unlike in the Landau paradigm, topological order, which is not attributed to symmetry breaking, is instead related to the Berry phase acquired by path-integrating through a closed adiabatic loop around a complex vector space defined by the Hamiltonian (e.g. bands in the Brillouin zone). One well-known topological effect, the quantum Hall effect [6, 1], is, itself, known to arise from time-reversal symmetry breaking by a strong magnetic field, which leads to a quantized Hall conductance associated with a topological invariant called a *Chern number*. [7] Here, the integral of the Berry curvature, which is given by the Berry phase around a small plaquette of infinitesimal area within the enclosed parameter space region divided by the area of that plaquette, over the occupied states described by the ground state Hamiltonian plus a perturbation to account for the application of a background electric field to generate current flow in a strong magnetic field leads to a nontrivial topological invariant, robust against disorder and

changes in material properties and device geometry. [8] It came as a surprise to many, then, that a topologically non-trivial system was predicted and observed for a system, not arising from symmetry breaking, but rather arising from symmetry protection. Specifically, these systems have a non-trivial \mathbf{Z}_2 topological classification. [9]

II.1. The \mathbf{Z}_2 Topological Insulator

The chalcogenide materials systems discussed in this chapter are distinguished by strong spin-orbit coupling associated with high Z-number of the elements composing the materials, which gives rise to band inversion at time-reversal (TR) symmetry protected point of high symmetry in the Brillouin zone (BZ). According to Kramers' theorem, for a TR -invariant Hamiltonian for spin- $1/2$ particles, all eigenstates are at least twofold degenerate [10]. In the absence of spin-orbit interactions, Kramers' degeneracy is simply the spin degeneracy. However, in the presence of spin-orbit interactions, a TR -invariant Hamiltonian, H , i.e. one that satisfies $\Theta H(\mathbf{k}) \Theta^{-1} = H(-\mathbf{k})$, can be classified by one of two topological classes defined by \mathbf{Z}_2 invariant ν : $\nu = 0$ or $\nu = 1$, signifying, respectively, a topologically trivial system and a topologically nontrivial system. [9, 11]

At the interface between two distinct systems, depending on the details of the Hamiltonian near the edge, there may or not exist band gap-crossing states bound to the edge of the shared interface of the two systems (for 2D topological insulators) or to the surface formed by the shared interface of the two systems (for 3D topological insulators). The minimum number N_K of Kramers pairs of edge modes intersecting the Fermi level, E_F , within the bulk band gap is given by the difference between the topological indices of the two systems according to $N_K = \Delta\nu \bmod 2$, an effect referred to as *bulk-boundary*

correspondence. [12] A system with an even number of Kramers pairs of edge modes that cross E_F can be smoothly deformed via an adiabatic transformation of the Hamiltonian to move all band-crossing edge modes out of the band gap. These states are *topologically equivalent*, i.e. $\nu_1 = \nu_2$. A system with an odd number of Kramers pairs of edge modes that cross E_F can never be smoothly transformed to reduce N_K below 1 without undergoing a topological phase change, revealing the topological protection of these states arising from the topological inequivalence of the two interfacing systems, i.e. $\nu_1 \neq \nu_2$.

The \mathbf{Z}_2 topological index, ν , can be calculated from a unitary matrix built from the occupied Bloch functions defined at four points in the bulk 2D Brillouin zone (for 2D topological insulators) or eight points in the bulk 3D Brillouin zone (for 3D topological insulators) where $+\mathbf{k}$ and $-\mathbf{k}$ coincide. These mathematical formulations are beyond the scope of this chapter, but can be studied in the following references. [9, 13, 14, 15, 16, 17, 18, 19, 20] In the following sections, the HgTe quantum well 2D topological insulator system and the V_2VI_3 -type $(\text{Bi,Sb})_2(\text{Se,Te})_3$ 3D topological insulator systems, hereby described as V_2VI_3 series systems, are introduced.

II.2. Mercury Telluride Quantum Wells

The type-III HgTe semiconductor quantum well is regarded as the first topological insulator to be studied. [21] Here, type-III refers to a heterojunction with a broken band gap that results from a distinctive inversion of the HgTe conduction and valence bands due to strong spin-orbit coupling. These materials systems consist of a thin HgTe sandwiched between two CdTe layers. CdTe is a topologically trivial (or “normal”) insulator with a bulk band gap of 1.5 eV, [22] whereas HgTe is topologically non-trivial due to the inversion of the

bands at the $k = 0$ point of the Brillouin zone driven by strong spin-orbit coupling. At HgTe quantum well thicknesses, d , below critical thickness, $d < d_c$, where d_c was found to be 6.4 nm, [23] the quantum well is dominated by the electronic structure of the CdTe layers, and the system is in the normal, topologically trivial, state. At HgTe quantum well thicknesses greater than the critical thickness, $d > d_c$, the quantum well is dominated by the inverted band structure of the HgTe, giving the highest occupied band of the electronic states within the well a Z_2 topological index of $\nu = 1$. The Z_2 topological index of the CdTe layers on either side of the HgTe quantum well, conversely, is a trivial $\nu = 0$. At the HgTe-CdTe interface, by the bulk-boundary correspondence described in the previous section, exists a pair of topologically protected helical edge states characterized by dissipationless spin current flow. These states describe a nontrivial topological phase called the quantum spin Hall (QSH) system, which is the hallmark topological effect in the HgTe quantum well system.

HgTe and CdTe have zincblende structure with space group $T_d^2 (F\bar{4}3m)$, a derivative of the diamond structure. These structures contain two symmetry-independent atomic sites per unit cell; cations Hg and Te occupy the Wyckoff 4a (0 0 0) positions in the cubic cell, and the Te anion occupies the Wyckoff 4c (0.25 0.25 0.25) position. The HgTe unit cell parameter is 6.462 Å, corresponding to a Hg-Te bond length of 2.797 Å, [24] and the CdTe unit cell parameter is 6.477 Å, corresponding to a Cd-Te bond length of 2.803 Å. [25] The interface between CdTe and HgTe experiences very little lattice strain, on the order of 0.2%. High quality barrier materials are often grown with the inclusion of Hg flux during growth, producing ternary alloy $Hg_xCd_{1-x}Te$ barrier layers. For example, König *et al.* observed the QSH effect in HgTe quantum wells sandwiched between topologically trivially insulating $Hg_{0.3}Cd_{0.7}Te$. [26]

The topologically nontrivial HgTe quantum well system is, necessarily, a layered heterostructure, and must therefore be synthesized in thin film form. Consequently, there is practically no bulk synthesis version of this materials system. The QSH effect has been demonstrated in HgTe quantum wells [23] grown by molecular beam epitaxy (MBE). [26] HgTe quantum well systems have also been synthesized by plasma-enhanced chemical vapor deposition (PECVD) [27] and metalorganic chemical vapor deposition (MOCVD), [28] albeit primarily for the purpose of producing infrared photodetectors rather than QSH insulators. These thin film growth techniques are described in section III. At a sufficient HgTe quantum well thickness $d > 6.4$ nm, measurements show a conductance plateau of close to $2e^2/h$, where e is the elementary charge and h is the Planck constant, that is independent of sample width, indicating it is caused by the predicted topological edge states. This seminal transport experiment is further discussed in section IV.

II.3. V_2VI_3 -series 3D Topological Insulators

V_2VI_3 -series topological insulator (TI) materials Bi_2Se_3 , Bi_2Te_3 , and Sb_2Te_3 have tetradymite rhombohedral crystal structure with space group D_{3d}^5 ($R\bar{3}m$) with five atoms per unit cell. [29] These materials form layered structures consisting of repeating layers of five lamellae, from which the structural identifier “quintuple layer (QL) structure” is derived. The lamellae of the QL are atomic planes arranged along the z-direction with the atomic composition of the lamella given by $X_1-M-X_2-M'-X_1'$, where X_1 , X_1' , and X_2 denote lamellae containing Se or Te atoms, and M , M' denote lamellae containing Bi or Sb atoms, with strong interatomic coupling of adjacent atoms within a QL and weaker coupling between QLs separated by van der Waals gaps. X_1 and X_1' are equivalent and M and M' are equivalent, with

the atoms of the top lamellae, X_1 and M , related to the atoms of the respective bottom lamellae, X_1' and M' , by an inversion operation in which the X_2 atoms act as inversion centers. The rhombohedral lattice parameters, Wyckoff positions, bond lengths, and interlamellar spacing of Bi_2Se_3 , Bi_2Te_3 , and Sb_2Te_3 are shown in Table 1.

Table 1. Rhombohedral lattice parameters, Wyckoff positions, bond lengths, and interlamellar spacing of Bi_2Se_3 , Bi_2Te_3 , and Sb_2Te_3 . M denotes Bi and Sb atoms and X denotes Se and Te atoms.

(a) Lattice parameters (\AA)			
	Bi_2Se_3 [30, 31]	Bi_2Te_3 [31]	Sb_2Te_3 [29]
a	4.14	4.39	4.26
c	28.6	30.5	30.5
(a) Wyckoff positions			
	Bi_2Se_3 [30, 31]	Bi_2Te_3 [31]	Sb_2Te_3 [29]
X_1	(0 0 0)	(0 0 0)	(0 0 0)
M	(0.2109 0.2109 0.2109)	(0.2097 0.2097 0.2097)	(0.2128 0.2128 0.2128)
X_2	(0.4006 0.4006 0.4006)	(0.4000 0.4000 0.4000)	(0.3988 0.3988 0.3988)
(c) Bond lengths (\AA)			
	Bi_2Se_3 [32]	Bi_2Te_3 [32]	Sb_2Te_3 [29]
$M-X_1$	2.97	3.04	2.98
$M-X_2$	3.04	3.24	3.17
X_1-X_1'	3.27	3.72	3.74
(d) Lamella spacing (\AA)			
	Bi_2Se_3 [30, 31]	Bi_2Te_3 [31]	Sb_2Te_3 [29]
d_{AB}	1.57	1.74	1.68
d_{BC}	1.93	2.03	2.00
$d_{CB'}$	1.93	2.03	2.00
$d_{B'A'}$	1.57	1.74	1.68
d_{vdW}	2.54	2.63	2.81

These TI materials exhibit a bulk band gap and band-crossing surface states supported by the non-trivial band topology of the topological insulator. Note that Sb_2Se_3 , which has an orthorhombic structure rather than a rhombohedral structure, is not a

topological insulator, but is, rather, a topologically trivial normal band insulator. Bi_2Se_3 has a direct bulk band gap at the Γ point of approximately 240 meV to 300 meV, [33] Bi_2Te_3 has an indirect bulk band gap of approximately 150 meV, [34] and Sb_2Te_3 has an indirect band gap of approximately 210 meV. [35] The topologically protected surface states are characterized by the electron spin locked perpendicular to the momentum (in the plane of the sample) related to the system's time reversal invariance that protects these conducting states against backscattering by non-magnetic impurities. Like HgTe, the topologically nontrivial nature of the occupied bands of these high Z-number V_2VI_3 -series materials is due to band inversion at the $\mathbf{k}=0$ point (the Γ point) of the Brillouin zone driven by strong spin-orbit coupling. The V_2VI_3 -series 3D topological insulator is distinct from the HgTe quantum well 2D topological insulator in that the former is characterized by four topological invariants, $(\nu_0; \nu_1\nu_2\nu_3) = (1; 000)$, where, at sufficient thickness of the V_2VI_3 layer, the primary topological index $\nu_0 = 1$ identifies the system as a strong topological insulator with symmetry protected surface states, and $\nu_1 = \nu_2 = \nu_3 = 0$, where $(\nu_1\nu_2\nu_3)$ can be interpreted as Miller indices describing the orientation of the layers, reveals that V_2VI_3 -series 3D topological insulator will not host time-reversal invariant topologically protected one-dimensional helical modes at the sites of any dislocations in the crystal. [36] The topological surface states of the V_2VI_3 -series materials appear in the band diagram as a band-gap-crossing surface state. Advantageously, the surface states in Sb_2Te_3 , Bi_2Se_3 , Bi_2Te_3 have been predicted to be nearly ideal single Dirac cone with near-linear energy-momentum dispersion [37], which has been experimentally demonstrated by angle-resolved photoelectron spectroscopy (ARPES) measurements to be the case for Bi_2Se_3 [38] and Bi_2Te_3 [38, 39]; due to a high level of intrinsic doping of naturally grown Sb_2Te_3 , the Fermi level of this material

lies in the bulk valence band continuum, below the surface states, and has, therefore, not been directly observed by using ARPES. A complication in studying the physics of carriers at the Dirac point of the surface states arises in Bi_2Te_3 as the Dirac point lies below the top of the BVB, signifying that studies of transport of the surface states at the Dirac point will be confounded by hole conduction in the BVB. Ternary and quaternary alloys of composition $\text{Bi}_{2-x}\text{Sb}_x\text{Se}_{3-y}\text{Te}_y$, with x and y tuned to achieve such alloys as BiSbTe_3 , $\text{Bi}_2\text{Se}_2\text{Te}$, and Bi_2SeTe_2 , may be synthesized to both adjust the position of the Dirac cone within the band gap, the charge type of the Dirac surface state charge carriers, and position the Fermi level within the bandgap to limit charge transport to the surface states. [40]

Experimentally, unlike the QSH state hosted by the HgTe quantum well system, the conductance of the topological surface states of the V_2VI_3 -series topological insulators is not characterized by a quantized conduction value, as these states are not dissipationless 1D chiral modes, but rather are a diffusive 2D electron system. However, due to the time-reversal symmetry of the system, the topological surface states are protected against direct backscattering by non-magnetic impurities. The spin texture of the topological surface states leads to highly spin-polarized current, motivating research of these materials for the development of spintronic applications. Furthermore, the interaction of the Dirac-like surface states with symmetry-breaking states, including those involved in ferromagnetic exchange and the Cooper pairs hosted by a superconductor, can produce exotic topological states. The quantum anomalous Hall effect (QAHE), observed when the time reversal symmetry of topological insulator surface states is broken by magnetic ordering induced by spontaneous magnetization, supports a quantized Hall conductance of e^2/h with a Chern number of 1. [41] Unlike the quantum Hall effect (QHE) described in Section II, the QAHE

arises spontaneously without inducement by an external magnetic field. Another example of an exotic topological state is the Majorana state hosted in topological superconducting systems, either bound to vortices in topological two-dimensional chiral p-wave superconductors [42] or as chiral Majorana modes in 1D chiral topological superconductors. [43] Experimental studies on these and other topological quantum states are discussed in Section IV.

III. Synthesis

This section briefly describes the thin-film growth techniques used to produce HgTe quantum well heterostructure materials and details the various bulk crystal growth, thin film growth, epitaxial deposition, and other techniques used to produce V_2VI_3 -series 3D topological insulators. An introduction to the various growth methods that have been demonstrated successfully to produce topological insulator chalcogenides, along with key growth method details, will be presented. Crystal quality is largely discussed in terms of structural and compositional characterization measurements, which will be described here.

III.1. Mercury Telluride Quantum Well Growth

The HgTe quantum well system is a trilayer CdTe/HgTe/CdTe heterostructure with an HgTe layer thickness of at least 6.4 nm. The CdTe layers in this heterostructure can be replaced with layers with composition $Hg_xCd_{1-x}Te$, where x is sufficiently small such that the layer preserves its topologically trivial non-inverted band gap. The epitaxial growth $Hg_xCd_{1-x}Te$ with very low x has is somewhat easier to produce with good crystallinity than pure CdTe because Cd incorporation is improved when growth is performed in a high Hg vapor

pressure environment, likely due to the prevention of tellurium precipitates. [44] The relative extent of Hg and Cd incorporation is tuned by the gas flow rates and substrate temperature.

The $\text{Hg}_x\text{Cd}_{1-x}\text{Te}/\text{HgTe}/\text{Hg}_x\text{Cd}_{1-x}\text{Te}$ system has been produced by means of several different layered heterostructure growth methods, including molecular beam epitaxy (MBE), vapor phase epitaxy (VPE) — including plasma enhanced chemical vapor deposition (PECVD), metalorganic VPE (MOCVD), and physical vapor deposition (PVD) — and liquid phase epitaxy (LPE). Laser assisted deposition and annealing have also been utilized to produce CdHgTe films [45]. Typically, a CdTe substrate is employed as a substrate, with different substrate surface conditions report to be best suited to growth by the different growth methods. A Cd-terminated CdTe(111) surface, also called a CdTe(111)A surface, for example, has been shown to be optimal for LPE growth. [46] A Te-terminated CdTe(111) surface, also called a CdTe(111)B surface, has been shown to be a suitable surface for MBE growth, [47] and CdTe(100) and CdTe(110) have both been shown to produce suitable CVD growth, [48, 49] but there is no well-established conclusion concerning the best orientation of the CdTe substrate for MBE or CVD growth.

Much of the early work on the synthesis and study of $\text{Hg}_{1-x}\text{Cd}_x\text{Te}/\text{HgTe}$ heterostructures was for the purpose of producing infrared detectors, although the linear zero-energy gap edge modes had been observed as early as 1983 in an MBE-grown HgTe-CdTe quantum well system. [50] Of the methods listed above, MBE is the favored method for producing abrupt interfaces between the HgTe layer and the trivial insulating CdTe.

Molecular beam epitaxy growth of HgTe quantum wells

The de facto method of producing high quality CdTe/HgTe/CdTe heterostructures with atomically abrupt CdTe-HgTe interfaces is molecular beam epitaxy, where molecular beams are generated under ultra-high vacuum conditions with beam intensities controlled by adjusting the temperatures of the effusion cells. Controlling effusion cell temperature (and thus elemental flux) and substrate temperature permits the highly controlled growth of epitaxial films with desired chemical compositions and CdTe/HgTe/CdTe quantum well structures with abrupt, smooth interfaces. While HgTe quantum well heterostructures can be grown by MBE on a number of substrates, including GaAs, [51, 52] InSb, [53] and Si, [54] optimal growth has been shown to occur on lattice-matched $\text{Cd}_{0.96}\text{Zn}_{0.04}\text{Te}$, which ensures minimal dislocation. [55]

MBE growth of these heterostructures requires low temperatures between 150 °C and 220 °C, [56, 57] with lower growth temperatures minimizing interdiffusion and demonstrating improved crystal quality. Growth occurs at very slow rates of around 1 $\mu\text{m/hr}$. The basic process entails generating molecular beams of desirable fluxes from Knudsen-type effusion cells under ultrahigh vacuum conditions by carefully controlling the temperature of the effusion cells. For the MBE growth of $\text{Hg}_{1-x}\text{Cd}_x\text{Te}$ using a metallic Hg vapor source, a metallic Cd source, and a Te_2 source, the Cd concentration, x , is primarily controlled by tuning the Cd/ Te_2 ratio. [58] The Hg vapor during growth has been shown to both prevent tellurium precipitates and contribute the Hg that incorporates at Cd-substitutional sites in the CdTe lattice. [44]

CVD growth of HgTe quantum wells

The growth of HgTe-CdTe superlattices by CVD on CdTe substrates has been shown to produce material of good quality at high growth rates by using a number of precursor reactants, including Cd precursor dimethylcadmium (DMCd); Hg precursors dimethylmercury (DMHg), HgI₂, and gaseous Hg in H₂ carrier gas; and Te precursors dimethyltelluride (DMTe) and diethyltelluride (DETe). Note that DMCd and DMHg are highly toxic; extreme care should be taken when working with these gases. Hg gas has been shown to be a workable substitute for DMHg if a lower-toxicity precursor is preferred. [59]

Hg_{1-x}Cd_xTe deposition with x very close to 1 occurs in the presence of DMHg at suitable gas flow rates and substrate temperatures during plasma-enhanced CVD growth such that Hg incorporation occurs to a negligible extent relative to Cd, as the high background vapor pressure of Hg precursor prevents tellurium precipitates. The thermodynamics of ternary alloy Hg_{1-x}Cd_xTe growth are complicated, as the growth is tuned by total pressure, substrate temperature, and the relative gas flows of DMTe/DETe, DMCd, DMHg/Hg, and H₂. An example plasma-enhanced CVD growth [27] of a HgTe layer occurs with a CdTe substrate heated to 150°C, 0.5 Torr system pressure, and carrier gas flow rates of 18 sccm (cm³/min) for DMTe and 20 sccm for DMHg. The slightly higher DMHg flow rate serves to reduce the incidence of Te precipitates. A CdTe layer is grown at a substrate temperature of 150°C with carrier gas flow rates of 2.4 sccm, 6 sccm, and 20 sccm for DMCd, DMTe, and DMHg, respectively. Note that in spite of the high flow rate of Hg precursor, Hg incorporation into Hg_{1-x}Cd_xTe is limited below 400°C, as only above this temperature does Hg begin to react with the Te alkyl. There is a strong temperature dependence of the Hg/Cd ratio, x , in Hg_{1-x}Cd_xTe. [60]

III.2. V_2VI_3 -series 3D Topological Insulators

Substantial research on chalcogenide topological insulator synthesis has been dedicated to understanding and controlling the growth to achieve suitable bulk electronic characteristics and to realize desirable surface-state-dominated electronic behaviors in these systems. [24] Synthesis of Bi_2Se_3 , both by bulk and thin film growth methods, often results in materials with strong n -type behavior arising from the high presence of selenium vacancies, which have a low energy of formation of approximately 500 meV and acts as a doubly positively charged vacancy contributing two conduction electrons to the system. Bi_2Te_3 tends to have weaker n -type behavior than Bi_2Se_3 due to a relatively lower concentration of tellurium vacancies, which have an energy of formation of approximately 600 meV, and a large concentration of singly ionized Bi'_{Te} antisite defects arising from the similar cation and anion electronegativities in Bi_2Te_3 that provide a single hole per antisite, somewhat offsetting the electron doping from Te vacancies. [61] Antisite defects are yet more pronounced in Sb_2Te_3 . The highly similar electronegativities between Sb and Te lead to an antisite energy of formation of only 350 meV, resulting in a very high concentration of Sb'_{Te} antisite defects — so high, in fact, that the synthesis of n -type Sb_2Te_3 has never been reported.

In addition to growth optimization, researchers have sought to produce exotic topological materials, such as magnetic topological insulators, which host the quantum anomalous Hall state described in Section II.3, and topological superconductors formed by imparting superconductivity on the topological edge or surface states by means of the

superconducting proximity effect or by growing superconducting doped topological insulators.

Synthesis of V_2VI_3 -series 3D topological insulator nanostructures

Synthesis of chalcogenide topological insulator nanostructures, such as nanoplatelets, nanowires, and nanoribbons, with controllable thickness has been demonstrated for several wet chemical synthesis and chemical vapor transport methods. Such methods are particularly useful for producing samples that enable investigation of physical behaviors as a function of sample size and thickness, and for producing samples of high crystalline quality. Example methods include polyol wet chemical synthesis of Bi_2Se_3 nanoplatelets, [62] high-yield solvothermal synthesis of Sb_2Te_3 nanoplatelets, [63] wire-like Sb_2Se_3 by hydrothermal reactions, [64] and Au-catalyzed vapor-liquid-solid (VLS) synthesis of Bi_2Se_3 nanowires in a horizontal tube furnace. [65, 66] Modifications can be made to these recipes to produce certain doped and alloyed versions of these nanostructures, such as using an Fe-Au catalyst instead of Au to produce magnetically doped Bi_2Se_3 nanoribbons by VLS synthesis. [67]

Bulk crystal growth of V_2VI_3 -series 3D topological insulators

Bismuth and antimony chalcogenide topological insulators can be grown by several bulk crystal synthesis techniques that produce single-crystal boules of material. The predominant bulk crystal growth method is the Bridgman furnace method. Bi_2Se_3 can be grown by a vertical Bridgman method with high-purity source materials of Bi:Se = 2:3 mixed in an argon-filled ampoule and heated to 770 °C for 15 hr, followed by a slow cooling of 1

°C/hr until the temperature reaches 615 °C, at which point the ampoule is quenched in room temperature water. [68] The growth of ternary alloy $\text{Bi}_{2-x}\text{Sb}_x\text{Se}_3$, optimized to achieve maximally suppressed bulk transport, was achieved by using the by sealing a mixture of pure elemental Bi, Sb, and Se with a nominal Bi:Sb:Se ratio of 52:7:130 in a quartz tube under Ar pressure; the ampoule was then heated to 740 °C over a period of 14 hr, held at 770 °C for 4 hr, cooled over a period of 50 hr to 550 °C, then held at 550 °C for 80 hr. [69] Incorporating other elements, such as Cu or Mn, during Bridgman synthesis has been demonstrated to produce, respectively, superconducting doped topological insulators [70] and magnetically doped topological insulators. [71]

V_2VI_3 -series 3D topological insulator thin films grown by molecular beam epitaxy

Unlike bulk crystal growth under equilibrium conditions, such as in a Bridgman single crystal growth furnace described above, MBE growth of Bi_2Se_3 , Bi_2Te_3 , Sb_2Te_3 , and related alloys allows the growth of monolithic crystalline structures with high crystalline perfection, tunable thickness, and arbitrary compositional profile, permitting careful doping, as well as the synthesis of V_2VI_3 -series 3D TI-based heterostructures, made possible by the precise atomic-layer-by-atomic-layer growth that characterizes the MBE method. For example, by using MBE, it is possible to produce heterostructures that consist of Bi_2Se_3 or Bi_2Te_3 layers separated by layers of ZnSe with arbitrary layer thickness as low as 10 Å [72], or Bi_2Se_3 or Bi_2Te_3 layers capped with a layer of Al or Se, or $\text{Bi}_{2-x}\text{Sb}_x\text{Se}_{3-y}\text{Te}_y$ alloys with tuned Bi:Sb and Se:Te ratios and doped with, for example, magnetic materials.

A generic MBE growth of V_2VI_3 -series chalcogenide samples typically involves the something resembling the following sequences. A substrate is deoxidized at temperatures

well above room temperature, e.g. 600 °C for GaAs (100). The growth of Bi₂Se₃ (Bi₂Te₃) is initiated by the deposition of a sequence of Se-Bi-Se-Bi-Se (Te-Bi-Te-Bi-Te) atomic layers at room temperature, after which the substrate is gradually heated to 300 °C to anneal the film to form the first quintuple layer (QL) of Bi₂Se₃ (Bi₂Te₃). MBE growth is performed under typical temperature, T , conditions of $T_{\text{Se}} (T_{\text{Te}}) < T_{\text{substrate}} < T_{\text{Bi}}$ for the effusion cell temperatures. Notably, the V₂VI₃-series chalcogenide TI materials, due to the interlayer van der Waals bonding mechanism for these layered materials, demonstrate rapid strain relaxation at the interface with a substrate, permitting the layers to grow in highly parallel fashion regardless of substrate composition and substrate growth surface orientation, as shown for GaAs (111) [73] and GaAs (100) substrates [74], Si substrates, [75] sapphire substrates, SrTiO₃ substrates [76], InP substrates, [77] etc.

Several methods have been shown to control the defect chemistry in V₂VI₃-series chalcogenides to tune the Fermi level to the bulk band gap (or, better yet, to the Dirac point of the surface states). These approaches fall primarily into the categories of compensation doping and optimizing the growth to eliminate the formation of vacancies and defects. Compensation doping takes advantage of the intrinsic doping tendencies arising from preferential formation of vacancies and antisites for the selected constituent anion and cation elements. For example, by growing a ternary alloy of Bi_{2-x}Sb_xTe₃, the n-type doping arising from naturally forming tellurium vacancies can be compensated by p-type doping contributions from Sb'_{Te} antisite defects. By tuning the Bi:Sb ratio, the position of the Fermi level can be correspondingly tuned. Brahlek et al. present a similar method of suppressing the bulk conducting states in Bi₂Se₃ by doping the alloy with Cu. [78]

Optimizing the growth of V_2VI_3 -series chalcogenide topological insulators demands the exploration of the boundless growth phase space, involving ascertainment of the optimal settings (typically specific to each individual growth system, no two ever being exactly alike) of growth parameters including growth temperature, growth chamber pressure, elemental beam flux ratios, choice of substrate, inclusion of a buffer layer prior to the main growth, and adequately sustaining low concentrations of unwanted reactants in the chamber. [79, 80, 81] Wang *et al.* have demonstrated reliable synthesis of high-quality Bi_2Se_3 by beginning sample growth by depositing a layer of a trivially insulating $(Bi_{1-x}In_x)_2Se_3$ buffer layer. [82] Walsh *et al.* present a Bi_2Se_3 growth methodology that allows for the tuning of the Fermi level through native doping in the binary alloy, demonstrating their growth of high-quality thin film Bi_2Se_3 with a mid-gap Fermi level by minimizing the Se vacancy concentration. [83]

IV. Experimental Investigations

Numerous experiments that have been devised to investigate the topological states hosted in topological insulators (TIs). These include spectroscopy measurements of the surface band structure, scanning tunneling microscopy measurements of the local density of states of the TI surface, and electrical transport measurements probing spin-polarization, time-reversal invariance, and quantization in topological edge and surface states. This section offers a brief overview of the experimental work that has revealed the novel electronic properties of topological states hosted in chalcogenide topological insulators.

IV.1. Spectroscopy

Several spectroscopy techniques have been applied to the study of topological insulators. These methods, which rely on the interaction between light and matter, reveal fundamental characteristics of the studied matter, including composition, physical structure, and electronic structure.

Photoemission spectroscopy experiments are principally based on the photoelectric effect discovered by Hertz [84] and described by Einstein. [85] Incident photons with energy greater than the work function ϕ of the material will expel electrons from the topmost atomic layers of the sample surface, with the energy of the expelled electrons given by $E_{kf} = h\nu - E_B - \phi$, where E_B is the binding energy of the electron, $h\nu$ is the known energy of the incident photon, and E_{kf} is the measured kinetic energy of the emitted electron. Two key photoemission spectroscopy methods that have provided key insights into topological insulator properties are x-ray photoemission spectroscopy (XPS), which elucidates the elemental and chemical state composition of the material surface, and angle-resolved photoemission spectroscopy (ARPES), which measures the density of single particle excitations in the reciprocal space of a solid, allowing for simultaneous measurement of both energy and momentum of electrons in the solid. By directly relating the kinetic energy of emitted electrons to both E_B and the crystal momentum $\hbar k$ of the solid to resolve occupied states in energy-momentum space, ARPES provides a unique capability of imaging the electronic band structures of materials. [86, 87]

Characterization of the electronic properties of chalcogenide 3D TI by XPS reveals significant information on surface oxidation, a common effect in chalcogenide compounds, [88, 89] and a generally undesirable one as oxides such as BiO_x and SeO_x do not support the

desirable topologically non-trivial properties of Bi_2Se_3 and other TIs. Atuchin *et al.* have shown success in fine-tuning bulk sample synthesis by using XPS to guide optimal synthesis techniques to produce chemically inert, non-oxidizing Bi_2Se_3 (0001) surfaces of excellent crystallographic quality. [90] In addition to surface compositional information, considerable analysis of the XPS spectra can also reveal compositional information of the bulk material. For example, by the measuring certain oxidation states, such as Mn oxidation states in Mn-doped Bi_2Se_3 , and comparing the differences in the amount of Se and Bi that precipitates out of the material as a function of Mn inclusion reveals the degree of disruption of the thermodynamic equilibrium of Bi_2Se_3 growth by the inclusion of Mn during synthesis. [91]

The topological surface states that had been theoretically predicted to exist at the surface of 3D TIs are depicted in the surface electronic band diagrams as helical Dirac-like band gap-crossing states with linear dispersion. Conveniently, ARPES is an ideal tool for directly measuring the surface band structure of samples of 3D TI candidate materials. Xia *et al.* compared first-principles calculations of the surface band structure of Bi_2Se_3 to ARPES measurements, matching the observation of a single Dirac cone of the surface state to that predicted as a characteristic signature of a topological insulator. [33] The position of the Dirac point of the Bi_2Te_3 surface state, which had been predicted by first-principles calculations to exist below the top of the bulk valence band, was confirmed by ARPES measurement to be about 0.13 eV below the top of the bulk valence band. [39] A study by Hsieh *et al.* showed that by combining spin-imaging with ARPES with a double Mott detector set-up, [92] the spin helicity of Bi_2Se_3 and Bi_2Te_3 can be directly resolved in the band diagram by ARPES. [38] Wang *et al.* performed similar measurement to observe the helical spin texture in Bi_2Se_3 by using a combination of ARPES and magnetic circular dichroism. [93]

In addition to probing the physics of 3D TIs as revealed in the surface band structure, is a powerful tool for assessing material quality. As discussed in the Synthesis section, the synthesis of nominally stoichiometric Bi_2Se_3 , Bi_2Te_3 , and Sb_2Te_3 is challenged by thermodynamic conditions during growth that lead to varying degrees of n-doping by the formation of Se and Te vacancies and p-doping by the formation of antisite defects. Ideally, the Fermi level for these binary alloy materials with stoichiometric compositions would be positioned within the band gap. The position of the Fermi level as measured by ARPES informs researchers the extent to which they must work to overcome undesirable n- and p-type doping to achieve the synthesis of 3D TI materials of desirable quality.

Raman spectroscopy is used to identify the structural fingerprints of solids by probing the vibrational, rotational, and other resonant modes of a crystalline system as a response to the inelastic scattering of incident visible, near-infrared, and near-ultraviolet monochromatic light. [94] This tool, in addition to providing structural characterization information, is useful technique for the investigation of phonons and electron-phonon interactions in systems with Dirac-like linear dispersion by means of such technique as double resonant Raman scattering, which has been used to measure the G and 2D modes in graphene. [95] This, in turn, offers a means of probing the coupling between charge carriers and Raman modes to monitor doping. [96] This technique has been employed to study how phonon properties, such as frequency and lifetime of the vibrational modes, in Bi_2Se_3 vary as a function of thickness from bulk to the atomically thin QL regime, revealing enhanced electron-phonon coupling in the few QL regime. [62] Similar results were revealed by micro-Raman study of few-QL flakes of Bi_2Se_3 , Bi_2Te_3 , and Sb_2Te_3 exfoliated from bulk material. [97] Investigation of the Raman scattering response of $\text{Cu}:\text{Bi}_2\text{Se}_3$ exfoliated from bulk material

measured in a quasi-backscattering geometry in various incident and scattered light polarization configurations reveals a strong temperature dependence of collision-dominated scattering of Dirac states at the Fermi level on bulk-valence states related to screening induced by thermally excited carriers. [98]

Other spectroscopy techniques that have been employed to study the unique characteristics of the topological surface states include terahertz spectroscopy and magneto-optical Kerr and Faraday spectroscopy. Terahertz spectroscopy using linearly polarized THz range electromagnetic radiation incident on a 3D TI of sufficiently good material quality with low crystalline disorder has been used to demonstrate a predicted Kerr rotation of the electromagnetic radiation's polarization plane [99] that is a signature of a topological magnetoelectric effect unique to these materials. [18] The Kerr rotation of reflected linearly polarized electromagnetic radiation, as well the related Faraday rotation that occurs for linearly polarized radiation transmitted through a sample, are also predicted to be observable with techniques using low frequency electromagnetic radiation. [100] Terahertz spectroscopy has also been used to reveal evidence of Dirac plasmons in Bi₂Se₃ micro-ribbon arrays. [101]

IV.2. Electrical Transport

Several key signatures of the non-trivial electronic properties of both HgTe QW 2D TIs and V₂VI₃-series 3D topological insulators can be probed by transport experiments. König *et al.* fabricated HgTe QW Hall bar devices and performed the transport experiment that showed the $2e^2/h$ quantized conductance, one conductance quantum for the top and

bottom edges of the quantum well, convincingly demonstrating the topological edge state transport of this 2D topological insulator. [23] For the V_2VI_3 3D TIs, while conventional magnetotransport measurements of resistivity and Hall mobility can be used to provide critical insight into material quality that drives improvements in synthesis techniques, [102, 81] distinguishing the transport of the topological surface states from that of the bulk bands is a major challenge. The synthesis of the materials leading to not quite stoichiometric composition, as discussed in the Synthesis section of this chapter, positions the Fermi level, not only away from the Dirac point, but often outside the bandgap. Furthermore, scattering events can occur during transport that cause conducting charges in the topological surface state to scatter into bulk states and vice versa. For this reason, probing the topological physics of the surface states of 3D TIs, requires synthesis of high-quality materials, clever adjustments to standard transport measurements, including fabricating device components that allow the adjustment of the position of the Fermi level by the application of a voltage to a gate terminal, [103] and rigorous analysis of transport data.

A notable property of the 2D surface states of the 3D TIs is the disallowance of direct backscattering by non-magnetic impurities due to time-reversal invariance. Consequently, the 2D topological surface states cannot be localized, even by strong disorder. [104] This leads to a contribution to the electrical conductivity in the form of weak antilocalization, a purely quantum mechanical phenomenon in which the destructive Aharonov-Bohm interference of two self-intersecting closed paths of scattered conducting charges reduces the probability of localized paths. [105] Results of separate studies by Chen *et al.* [106] and Checkelsky *et al.* [107] on Bi_2Se_3 and He *et al.* on Bi_2Te_3 [108] substantiate the predicted relationship between weak antilocalization and the topologically protected surface states.

Another quantum transport phenomenon observed in 3D TIs is the Shubnikov-de Haas (SdH) effect, which manifests as an oscillation in the conductivity at high magnetic fields associated with Landau level occupation and has a period of $1/|B|$, where $|B|$ is the magnitude of the applied magnetic field, from which the carrier concentration can be derived. [109] Additionally, analysis of the temperature dependence of the SdH oscillations reveals the effective mass of the high mobility charge carriers participating in the SdH effect. [110] Analytis *et al.* show that when the Fermi level lies within the Bi_2Se_3 bulk conduction band, the SdH oscillations are dominated by bulk transport, and the effective cyclotron mass derived from analysis of the SdH oscillations match well with the effective mass calculated from the parabolic fit to the band dispersion of the ARPES-measured conduction band. [111] Qu *et al.* [112] and Ren *et al.* [113] show that when the Fermi level is positioned well within the bulk band gap for Bi_2Te_3 and $\text{Bi}_2\text{Te}_2\text{Se}$, respectively, the SdH oscillations come from the topological surface states.

The spin-momentum locking of the topological edge and surface state carriers can be observed by measuring the spin-polarization of the transported charges, injected as an unpolarized bias current, at magnetic tunnel barrier surface contacts. A study by Brune *et al.* on HgTe QW 2D TIs, in which the HgTe QW sample was fabricated into a split-gate H-bar device, combined quantum spin Hall (topologically non-trivial) and metallic spin Hall (topologically-trivial) transport in a single device to show that the quantum spin Hall effect can be used as a spin current injector and detector for the metallic spin Hall effect, establishing the spin polarization of the helical edge states in HgTe QW 2D TIs purely by means of an electrical transport. [114] The spin-polarization of the 3D TI Bi_2Se_3 surface current was detected by Li *et al.* by using magnetic tunnel barrier surface contacts as spin

detectors, where the voltage measured by the magnetic tunnel barrier surface contact depends on the orientation of the contact magnetization, showing a lower voltage when the orientations of the spin-polarization of the current and the magnetization of the magnetic tunnel barrier contact are aligned. [115, 116] The spin-polarized 3D TI surface states have been shown to provide efficient spin-orbit induced torques on magnetic layers adjacent to the TI via the Rashba-Edelstein effect, [117, 118] exerting strong spin-transfer torques, even at room temperature, on adjacent ferromagnetic permalloy layers such as Ni₈₁Fe₁₉ [119] and Co₄₀Fe₄₀B₂₀. [120]

IV.3. Exotic topological states

Quantum anomalous Hall effect

The quantum anomalous Hall state occurs when the time-reversal symmetry of the topological surface state is broken by spontaneous magnetization induced by proximity effect from an interfacing ferromagnetic system or by magnetic dopant-induced magnetization in the topological insulator material, itself, hosting a topologically protected edge mode with a Chern number of one corresponding to a quantized Hall conductance of e^2/h . The quantum anomalous Hall effect has been predicted for both magnetically doped HgTe [121] and for (Bi,Sb)₂(Se,Te)₃ systems [122] with induced magnetization, but has thus far been observed only convincingly in the latter. The challenge in observing the QAH effect in HgTe quantum wells arises largely due to the exchange field in Mn-doped HgTe quantum wells being insufficiently strong to produce ferromagnetic ordering, even at very low temperatures, preventing the spontaneous magnetization necessary to break the time

reversal symmetry of the topological edge modes without a persistent external magnetic field to paramagnetically align the Mn spin moments. On the other hand, in magnetically-doped $(\text{Bi,Sb})_2(\text{Se,Te})_3$ systems, spontaneous magnetization is induced by a strong van Vleck mechanism. [123] Van Vleck paramagnetism produces considerable spin susceptibility without the need for itinerant charge carriers to mediate magnetic exchange, as is the case for the Ruderman-Kittel-Kasuya-Yosida (RKKY) exchange mechanism in conventional diluted magnetic semiconductors such GaMnAs. [124] This has the significant advantage of excluding additional conduction channels in the topological insulator bulk. In a high-quality magnetically doped $(\text{Bi,Sb})_2(\text{Se,Te})_3$ material system, when the Fermi level is tuned to the magnetic gap in the Dirac cone, this would limit current to flow through the quantum anomalous Hall chiral edge state.

A robust QAH state has been observed in magnetically doped 3D TI alloys of several different compositions. Below the Curie temperature, with out-of-plane oriented magnetization and at zero magnetic field, the signature of the QAH effect is a Hall conductance σ_{xy} of precisely e^2/h and zero longitudinal resistance. The QAH has been successfully observed in Cr-doped $(\text{Bi,Sb})_2\text{Te}_3$ [41, 125] and V-doped $(\text{Bi,Sb})_2\text{Te}_3$, the latter of which was shown to support a Hall conductance of $0.9998 \pm 0.0006 e^2/h$ and a zero-field longitudinal resistance of $0.00013 \pm 0.00007 h/e^2$ At 25mK. [126]

Topological superconductors

Direct proximity to an s -wave superconductor gives rise to a topological two-dimensional chiral p -wave superconductor at the superconductor/topological insulator

(SC/TI) interface when the Cooper pairs tunnel into the topological surface states and induce a superconducting energy gap in the Dirac cone. [127] Such experimentally accessible topological superconductors were proposed by Fu and Kane, [128] and signatures of superconducting proximity effect have been observed in numerous SC/TI systems NbSe₂/Bi₂Se₃, [129, 130] NbSe₂/Bi₂Te₃, [131] W/Bi₂Se₃, [132] In/Bi₂Te₃, [133] and others. Superconductivity has also been demonstrated in superconducting doped topological insulators such as Cu:Bi₂Se₃. [70, 134]

Topological superconductivity can be induced in topological surface states by the generation of supercurrent between two superconducting contacts at the edge of a 2D TI or the surface of a 3D TI via the Josephson effect. [135] The Josephson effect for a superconductor/2D TI (eg. HgTe QW)/superconductor junction has been predicted to produce a fractional Josephson effect with a current-phase relationship with 4π periodicity, which is half the usual 2π periodicity in the non-topological Josephson effect. [136] The signature 4π periodicity of the Josephson supercurrent has been demonstrated in HgTe QW-based Josephson junction devices as missing odd-integer-index ($n=1, 3, 5$, etc.) Shapiro steps in the response of a Josephson junction to rf radiation. [137] This has also been observed in Bi₂Se₃-based Josephson junctions as a missing $n=1$ Shapiro step. [138]

Topological superconductivity shares with conventional superconductivity several essential signatures, the most straightforward of which is zero electrical resistance below the Curie temperature, T_c . Furthermore, a superconducting gap is measurable as a pronounced dip in the density of states, which can be measured locally by scanning tunneling spectroscopy. Unfortunately, the direct measurement of evidence of the formation of the

exotic superconducting condensates of the topological surface states is confounded by the fact that the bulk states of the material system are also superconducting. While superconductivity and topological order can be independently observed in a single material system, [70, 130] the unique signature of topological superconductivity is the existence of topologically protected zero-energy quasiparticle states called *Majorana modes* that exist at the physical boundary of the topological superconductor. [128]

Majorana fermions

The zero energy Majorana modes exist at the physical boundaries of topological superconductors as either bound Majorana zero modes or as chiral Majorana modes. [12] The Majorana fermion can be imagined as a half of the ordinary Dirac fermion of the topological edge (surface) mode of the 2D TI (3D TI). Moreover, due to the particle-hole redundancy of these particles, they carry no charge and are their own antiparticle. [139] Majorana modes are always created in pairs, that when physically separated, define a degenerate two-level system whose overall quantum state is stored nonlocally, a property that motivates research to explore using Majorana modes for quantum information processing. [140]

A pair of Majorana zero modes appear at the two ends of a 1D topological superconducting wire of finite length, which is formed by inducing superconductivity in the edge modes of a 2D TI such as an HgTe QW. The signature of the Majorana zero mode is a zero-bias differential conductance peak indicating a bound Andreev state within the superconducting gap, actual measured differential conductance of which will depend on the

conditions of the experiment. [141] The signature zero-bias differential conductance peak has been observed in InSb nanowires contacted by a superconducting NbTiN electrode, supporting the hypothesized existence of Majorana zero modes in this system. [142] It should be noted, however, that these differential conductance peaks also appear for topologically trivial Andreev bound states, and it can be difficult to distinguish topologically nontrivial Majorana bound states from topologically trivial Andreev bound states in a differential conductance measurement. [143] While the Majorana zero mode signature zero-bias peak has not yet been observed in HgTe QW-based systems, the 4π periodic supercurrent in HgTe QW-based topological Josephson junctions, which has been theoretically shown to be a signature of the existence of topological gapless Andreev bound states, [136] has been observed in these systems. [144]

Propagating chiral Majorana modes exist either in the cores of superconducting vortices [145] or along the physical edge of a quantum anomalous Hall system with induced superconductivity, [146, 147] observed in a quantum anomalous Hall insulator/topological superconductor Hall bar device fabricated from a $(\text{Cr}_{0.12}\text{Bi}_{0.26}\text{Sb}_{0.62})_2\text{Te}_3$ grown on GaAs (111)B by molecular beam epitaxy with a Nb superconductor bar deposited across the center of the Hall bar. [148] The unique signature of the chiral Majorana mode, provided the two Majorana fermions are sufficiently well separated such that the dephasing length is greater than the superconducting coherence length, is a half-integer Hall conductance plateau of $\frac{1}{2}e^2/h$. [149]

V. Summary and Outlook

Research on chalcogenide topological insulators has, thus far, established the basic properties of these materials systems and made measurable progress in the developing good synthesis methods and measurement techniques that probe the unique physics of topological insulators. Substantial effort is yet required, however, to realize the full potential of these materials in terms of materials quality and applications.

As of the publication of this text, a number of promising devices based on chalcogenide topological insulator (TI) materials are in the development pipeline. Several devices fall in the category of spintronics devices, making use of the topologically protected spin texture of the surface states to perform such functions as conduct coherent spin information along TI interconnects or control spin moments in thin magnetic films by means of the spin transfer torque (STT) effect described in Section IV to control memory states. Other devices are topological quantum computing devices that utilize Majorana fermions — either bound modes or chiral modes, depending on the design of the system — as the building blocks for topological qubits.

Going forward, researchers will continue to find a vast investigative space to study new and improved synthesis techniques to grow HgTe QW structures and $(\text{Bi,Sb})_2(\text{Se,Te})_3$ -based materials, develop and utilize sensitive measurements to probe their rich physics, and innovate next generation sensors and electronic devices. In addition, other unique physical phenomena will emerge in topologically non-trivial systems produced from chalcogenide topological insulator-based alloys and heterostructures, requiring the exploration of a boundless parameter space of compositions, growth conditions, device designs, and field effects. Moreover, these materials offer an exciting materials platform to better understand topological aspects of physical systems. In conclusion, researchers in the intersecting fields

of chemistry, materials science, physics, and engineering can look forward to many exciting advances and new directions in the study of chalcogenide topological insulators.

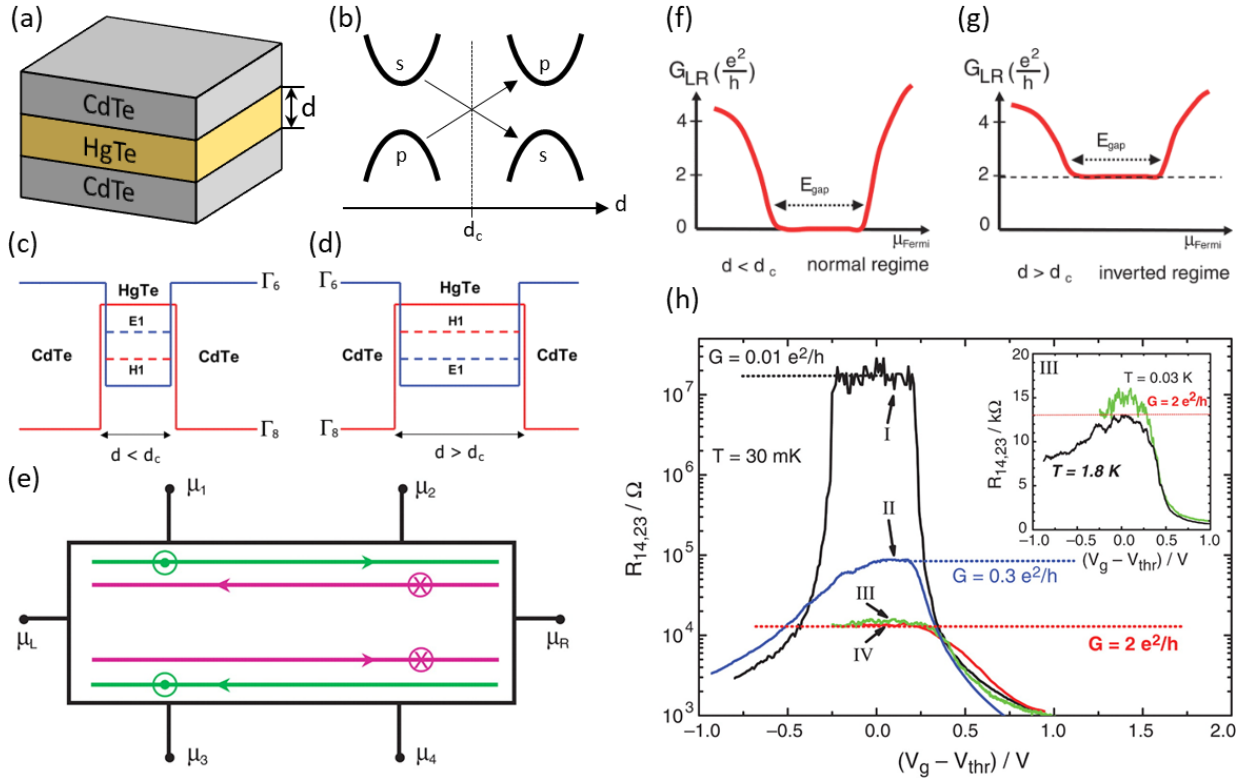


Figure 1. The quantum spin Hall effect (QSHE) in HgTe quantum well (QW) 2D topological insulators. a) CdTe/HgTe/CdTe quantum well structure; d is the thickness of the HgTe QW layer. b) The QW subbands undergo an inversion from a normal regime, with a valence band with p-type character and a conduction band with s-type character, to an inverted regime, with a valence band with s-type character and a conduction band with p-type character, for HgTe layer thicknesses greater than a critical thickness, $d > d_c$, where $d_c = 6.4$ nm. This effect arises from the inverted band structure of HgTe and the normal band structure of the CdTe barrier layers. c) For $d < d_c$, the band structure of the CdTe layers dominate within the QW, and the s-type E1 quantum well subband lies above the p-type H1 subband (normal regime); d) for $d > d_c$, the band structure of the HgTe dominates within the QW, and the s-type E1 QW subband lies below the p-type H1 subband (inverted regime). e) The spin-polarized topological edge states of the QSHE. f) In the normal regime for a HgTe QW ($d < d_c$), the two-terminal conductance will vanish when the Fermi level is positioned within the bulk band gap of the QW. g) The experimental signature of the QSHE effect in the inverted regime for a HgTe QW is a quantized $2e^2/h$ two-terminal conductance when the Fermi level is positioned within the bulk band gap of the QW. h) Quantized $2e^2/h$ two-terminal conductance was experimentally observed for HgTe QW devices with HgTe layer thickness greater than d_c (samples III and IV); sample I has a HgTe QW thickness less than d_c and, consequently, demonstrates normal insulating behavior. Figs. 1c–g are adapted from Bernevig *et al.* [21] Fig. 1h is adapted from König *et al.* [23]

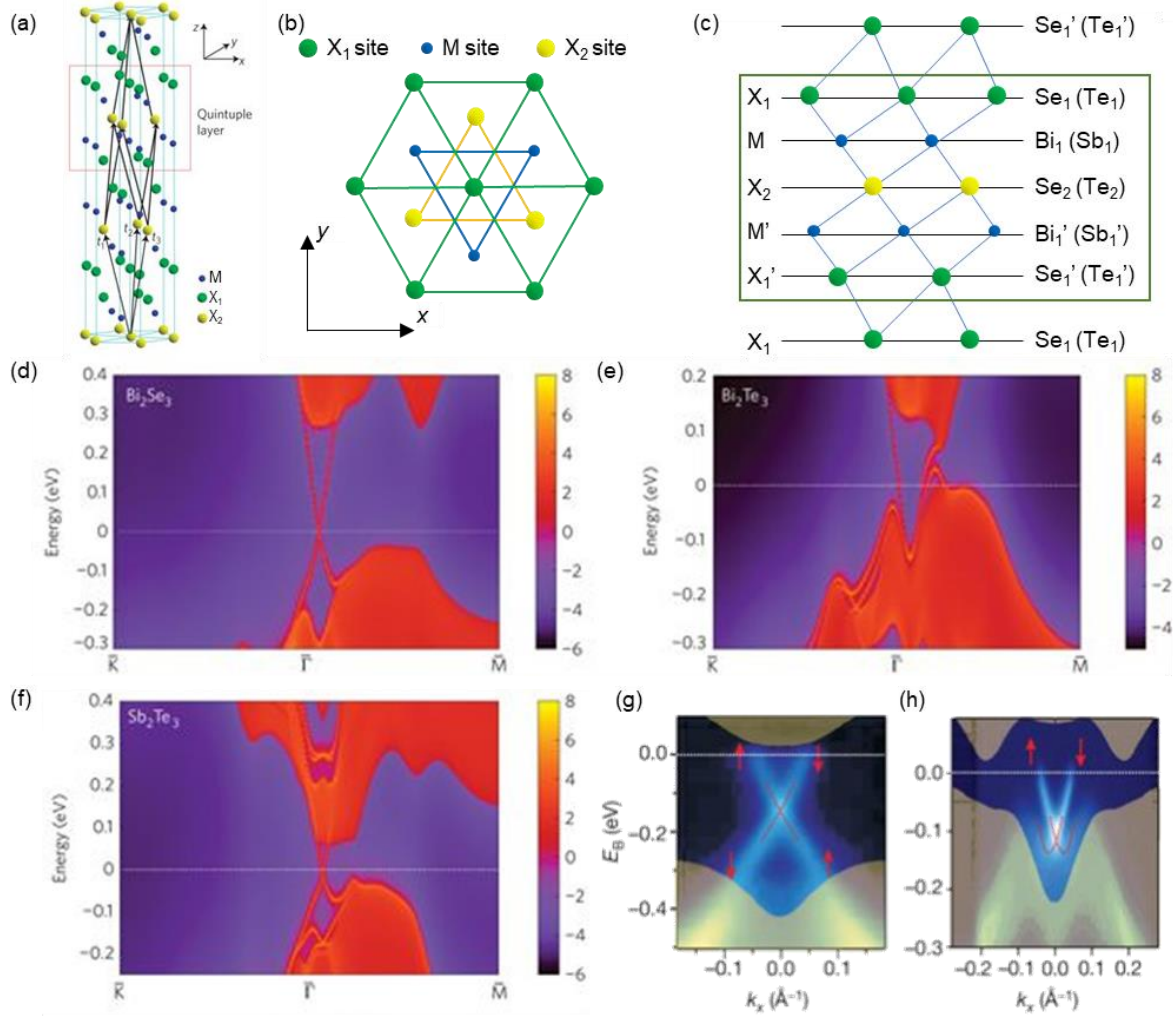


Figure 2. 3D topological insulators Sb_2Te_3 , Bi_2Se_3 , and Bi_2Te_3 . a) Side view of the quintuple layer structure of Sb_2Te_3 , Bi_2Se_3 , and Bi_2Te_3 , with the three primitive lattice vectors t_1 , t_2 , and t_3 and lattice sites M (Sb, Bi) and X_1 and X_2 (Se, Te) labeled. b) Top view of the Sb_2Te_3 , Bi_2Se_3 , and Bi_2Te_3 structure along the z -direction. c) Side view of the Sb_2Te_3 , Bi_2Se_3 , and Bi_2Te_3 structure showing the stacking of atomic lamellae along the z -direction. d–f) Energy-momentum band dispersion along $\bar{K}-\bar{\Gamma}-\bar{M}$ for Bi_2Se_3 (d), Bi_2Te_3 (e), and Sb_2Te_3 (f). g–h) Angle-resolved photoemission spectroscopy (ARPES)-measured band dispersion of Bi_2Se_3 (g) and Bi_2Te_3 (h) (111) surfaces in the vicinity of the $\bar{\Gamma}$ point of the 2D Brillouin zone along $\bar{K}-\bar{\Gamma}-\bar{M}$, revealing the topological surface states. Fig. 2a–f are adapted from Zhang *et al.* [37] Figs. 2g–h are adapted from Hsieh *et al.* [38]

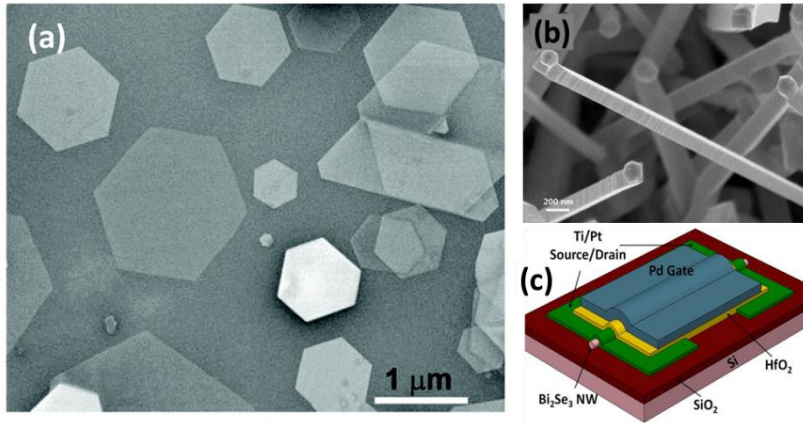


Figure 3. Bi₂Se₃ nanoplatforms (a) and nanowires (b). Schematic of a Bi₂Se₃ nanowire field effect transistor. Fig. 3a adapted from Zhang *et al.* [62] Fig. 3b-c adapted from Zhu *et al.* [65]

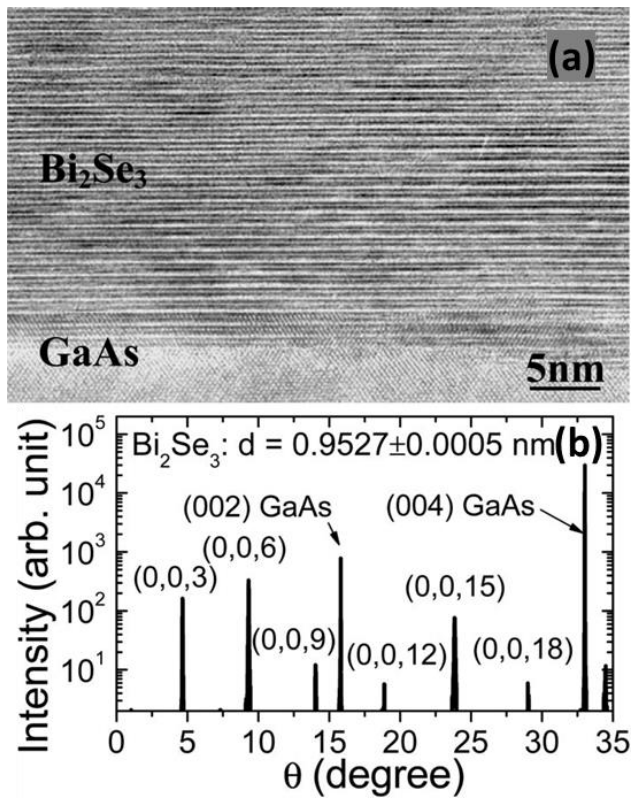


Figure 4. a) Transmission electron microscopy cross sectional image and (b) x-ray diffraction pattern of Bi_2Se_3 grown by molecular beam epitaxy on GaAs (100) substrate adapted from Liu *et al.* [74]

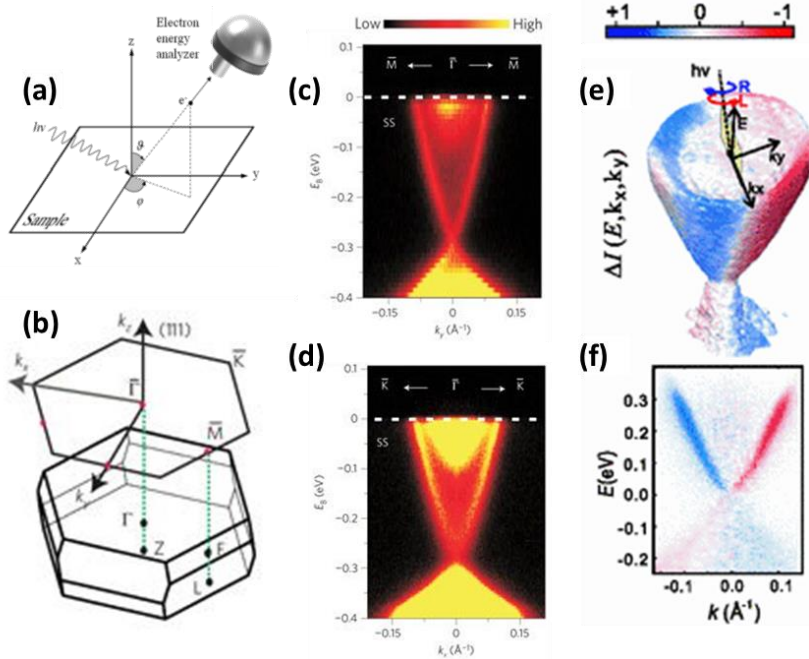


Figure 5. a) ARPES experimental apparatus schematic. Emitted photoelectron energies are characterized by a finite acceptance angle in the angle-resolved electron energy analyzer, and parallel and perpendicular components of the momentum are determined from the polar (ϑ) and azimuthal (ϕ) emission angles. b) A schematic diagram of the Bi_2Se_3 bulk three-dimensional Brillouin zone and the two-dimensional Brillouin zone of the projected (111) surface. c–d) ARPES measurements of the Bi_2Se_3 (111) band dispersion, including the gapless surface bands, near the $\bar{\Gamma}$ point of the 2D Brillouin zone along $\bar{M}-\bar{\Gamma}-\bar{M}$ (c) and along $\bar{K}-\bar{\Gamma}-\bar{K}$ (d). e) Time-of-flight-ARPES data for all momentum directions measured using right- and left-circularly polarized light showing the spin texture of the electronic surface bands. f) A slice of the data in (e) showing the spin polarization of the surface states in the energy-momentum map of Bi_2Se_3 (111) near the $\bar{\Gamma}$ point of the 2D Brillouin zone along $\bar{M}-\bar{\Gamma}-\bar{M}$. Fig. 5b–d adapted from Xia *et al.* [33] Fig. 5e–f adapted from Wang *et al.* [93]

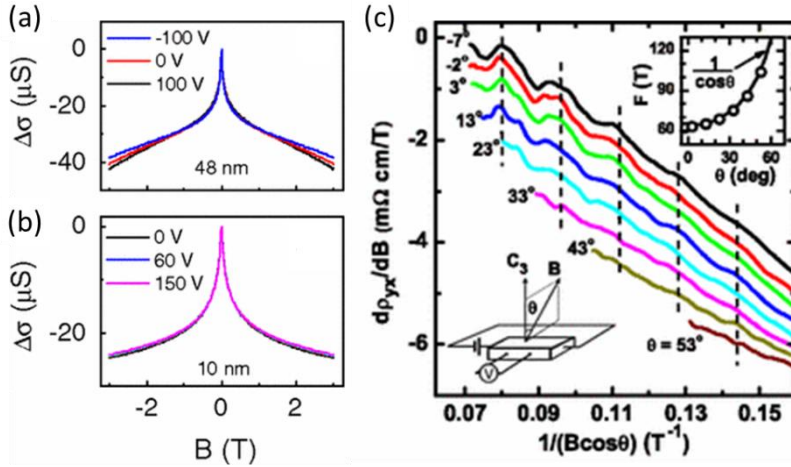


Figure 6. a–b) The contribution to conductivity due to weak localization for a 48 nm sample of Bi_2Se_3 (a) and a 10 nm sample of Bi_2Se_3 (b) grown on SrTiO_3 with various voltages applied to a back gate, demonstrating very little gate-voltage dependence of the weak antilocalization signal. C) The derivative of the Hall resistivity of a bulk-grown $\text{Bi}_2\text{Te}_2\text{Se}$ cleaved single crystal sample with respect to the magnetic field as function of the perpendicular component of the magnetic field, B_{\perp} , at various angles of the magnetic field with respect to $\text{Bi}_2\text{Te}_2\text{Se}$ crystalline c -axis. The $1/B_{\perp}$ periodicity of the oscillations indicates the existence of a well-defined two-dimensional Fermi surface. Figs. 6a–b are adapted from Chen *et al.* [106] Fig. 6c is adapted from Ren *et al.* [113]

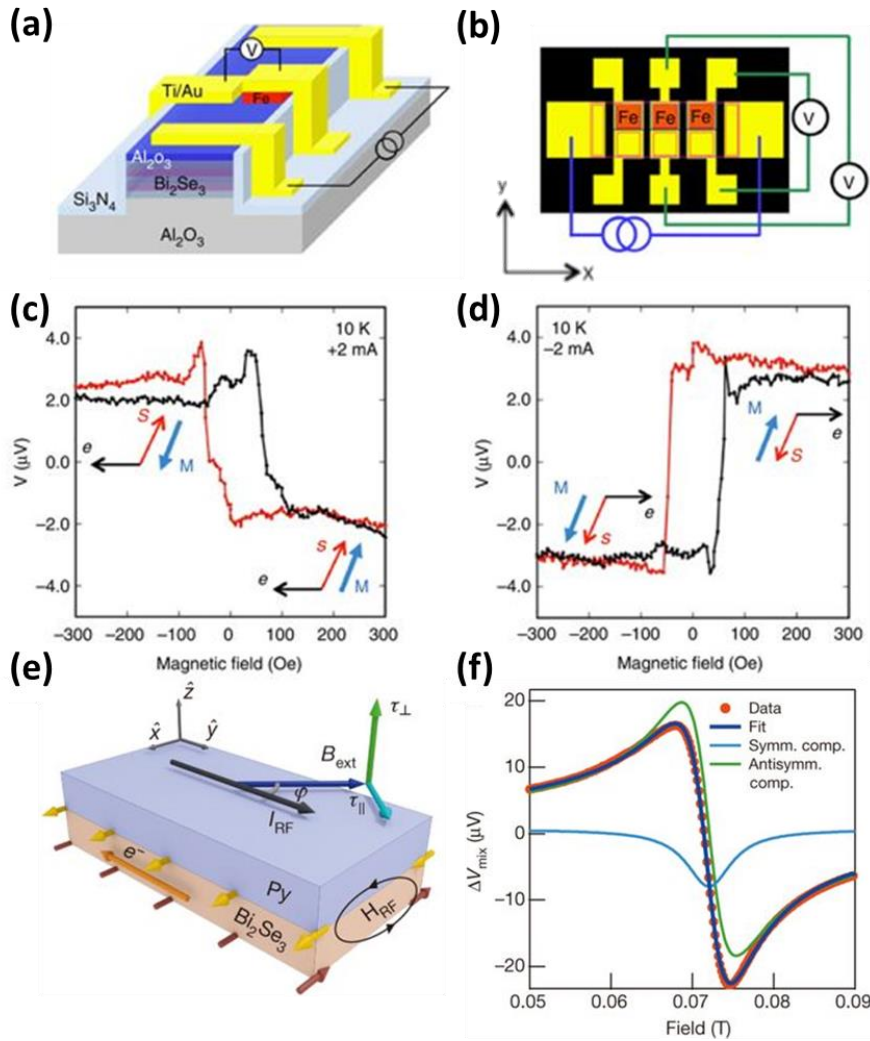


Figure 7. Schematic (a) and top view (b) of the contact layout for a spin polarization detection method in Bi_2Se_3 , with parallel rows of ferromagnetic Fe contacts (top row, red) and non-magnetic Ti/Au reference contacts (bottom row, yellow). The magnetic field dependence of the voltage measured at the ferromagnetic spin detector contact with the contact magnetization parallel to the topological surface state spin for bias currents of +2mA (c) and -2mA (d), revealing significantly lower detector voltages when the Fe contact magnetization is aligned with topological surface state spin. e) Schematic diagram of the Bi_2Se_3 /permalloy layer structure for measuring spin transfer torque produced by the spin-polarized topological surface states exerted on the magnetic moments of the permalloy, revealed by spin-torque ferromagnetic resonance experiment (f). Figs. 7a–d are adapted from Li *et al.* [116] Figs. 7e–f are adapted from Mellnik *et al.* [119]

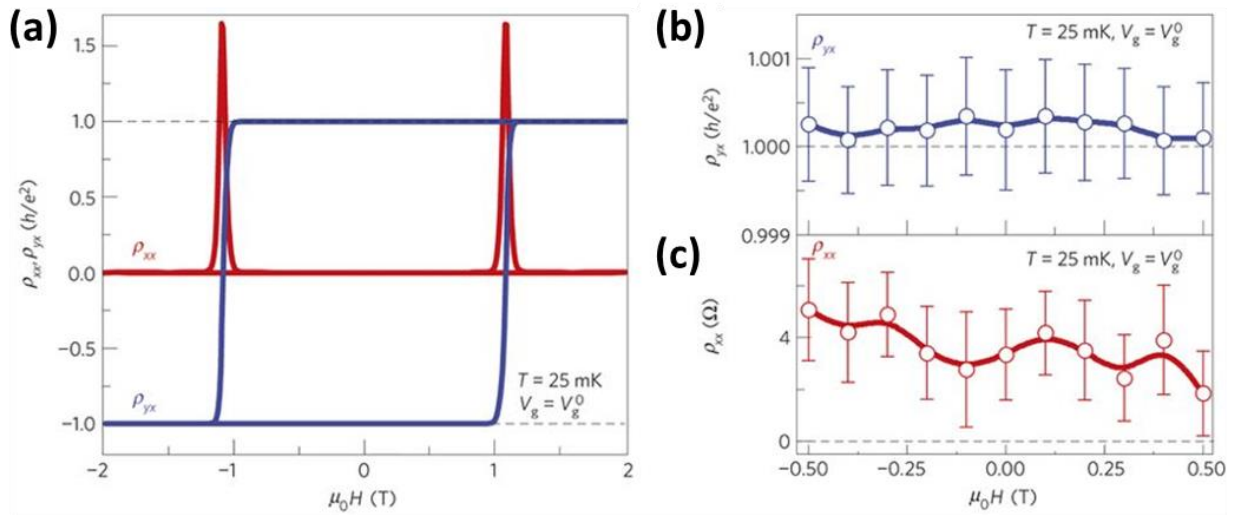


Figure 8. The quantum anomalous Hall effect (QAHE). a) The magnetic field dependence of the longitudinal resistivity ρ_{xx} and the Hall resistance ρ_{yx} of four-quintuple-layer of an MBE-grown $(\text{Bi}_{0.29}\text{Sb}_{0.71})_{1.89}\text{V}_{0.11}\text{Te}_3$ film on SrTiO_3 substrate reveals, within one standard deviation the signature zero-field h/e^2 quantized Hall resistance (b) and, within approximately two standard deviations, the expected zero resistance at zero magnetic field (c). Figs. 8a–c adapted from Chang *et al.* [126]

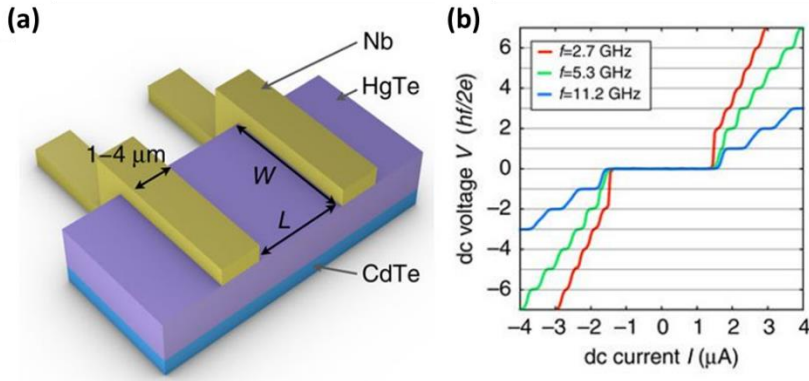


Figure 9. a) Schematic of Josephson junction device with Nb contacts patterned on HgTe mesa stripes grown on CdTe substrate. b) Shapiro steps are observable in the I - V curve for a Josephson junction system in the presence radio frequency radiation, shown here for three different frequencies measured at $T \approx 800$ mK. The first Shapiro step is reduced for $f = 5.3$ GHz and is fully suppressed for $f = 2.7$ GHz. Figs. 9a–b are adapted from Wiedenmann *et al.* [137]

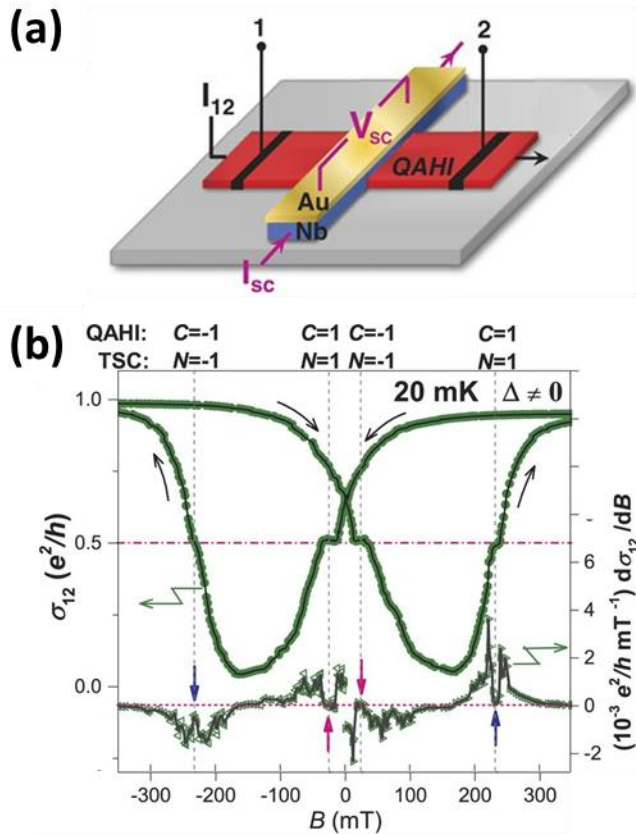


Figure 10. Electrical transport measurement of chiral Majorana fermion signature. a) Schematic of a topological superconducting device consisting of a quantum anomalous Hall insulator (QAHI), a 6nm-thick $\text{Cr}_{0.12}\text{Bi}_{0.26}\text{Sb}_{0.62})_2\text{Te}_3$ thin film grown on a GaAs(111) substrate by molecular beam epitaxy, and a Nb superconductor bar. A current is applied along the QAHI and the four terminal longitudinal conductance σ_{12} is measured from the potential drop across terminals 1 and 2. b) σ_{12} as a function of magnetic field shows the half-integer $e^2/2h$ conductance plateaus signifying the existence of single chiral Majorana edge modes. Figs. 10a–b are adapted from He *et al.* [148]

References

- [1] D. J. Thouless, M. Kohmoto, M. P. Nightingale and M. den Nijs, "Quantized Hall Conductance in a Two-Dimensional Periodic Potential," *Physical Review Letters*, vol. 49, p. 405, 1982.
- [2] X.-G. Wen, "Topological orders and edge excitations in fractional quantum Hall states," *Advances in Physics*, vol. 44, pp. 405-473, 1995.
- [3] L. Landau, "On the Theory of Phase Transitions," *Journal of Experimental and Theoretical Physics*, vol. 7, pp. 19-32, 1937.
- [4] W. A. Bardeen, C. T. Hill and M. Lindner, "Minimal dynamical symmetry breaking of the standard model," *Physical Review D*, vol. 41, p. 1647, 1990.
- [5] D. Forster, *Hydrodynamic Fluctuations, Broken Symmetry, And Correlation Functions*, Reading, MA: W. A. Benjamin, 1975.
- [6] F. D. M. Haldane, "Model for a Quantum Hall Effect without Landau Levels: Condensed-Matter Realization of the "Parity Anomaly"," *Physical Review Letters*, vol. 61, pp. 2015-2018, 1988.
- [7] M. Nakahara, *Geometry, Topology and Physics*, Bristol: Hilger, 1990.
- [8] B. I. Halperin, "Quantized Hall conductance, current-carrying edge states, and the existence of extended states in a two-dimensional disordered potential," *Physical Review B*, vol. 25, pp. 2185-2190, 1982.
- [9] C. L. Kane and E. J. Mele, "Z₂ Topological Order and the Quantum Spin Hall Effect," *Physical Review Letters*, vol. 95, p. 146802, 2005.
- [10] H. A. Kramers, "Théorie générale de la rotation paramagnétique dans les cristaux uniaxes de terres rares," *Proceedings of the Royal Netherlands Academy of Arts and Science*, vol. 33, pp. 959-972, 1930.
- [11] C. L. Kane and E. J. Mele, "Quantum Spin Hall Effect in Graphene," *Physical Review Letters*, vol. 95, p. 226801, 2005.
- [12] M. Z. Hasan and C. L. Kane, "Colloquium: Topological insulators," *Reviews of Modern Physics*, vol. 82, pp. 3045-3067, 2010.
- [13] C. L. Kane and L. Fu, "Time reversal polarization and a Z₂ adiabatic spin pump," *Physical Review B*, vol. 74, p. 195312, 2006.

- [14] C. L. Kane and L. Fu, "Topological insulators with inversion symmetry," *Physical Review B*, vol. 76, p. 045302, 2007.
- [15] T. Fukui and Y. Hatsugai, "Quantum Spin Hall Effect in Three Dimensional Materials: Lattice Computation of Z₂ Topological Invariants and Its Application to Bi and Sb," *Journal of the Physical Society of Japan*, vol. 76, p. 053702, 2007.
- [16] J. E. Moore and L. Balents, "Topological invariants of time-reversal-invariant band structures," *Physical Review B*, vol. 75, p. 121306(R), 2007.
- [17] T. Fukui, T. Fujiwara and Y. Hatsugai, "Topological Meaning of Z₂ Numbers in Time Reversal Invariant Systems," *Journal of the Physical Society of Japan*, vol. 77, p. 123705, 2008.
- [18] X. L. Qi, T. L. Hughes and S. C. Zhang, "Topological field theory of time-reversal invariant insulators," *Physical Review B*, vol. 78, p. 195424, 2008.
- [19] R. Roy, "Z₂ classification of quantum spin Hall systems: An approach using time-reversal invariance," *Physical Review B*, vol. 79, p. 195321, 2009.
- [20] Z. Wang, X. L. Qi and S. C. Zhang, "Equivalent topological invariants of topological insulators," *New Journal of Physics*, vol. 12, p. 065007, 2010.
- [21] B. A. Bernevig, T. L. Hughes and S. C. Zhang, "Quantum spin Hall effect and topological phase transition in HgTe quantum wells," *Science*, vol. 314, p. 1757, 2006.
- [22] D. R. Lovett, *Semimetals and narrow-bandgap semiconductors*, London: Pion Ltd., 1977.
- [23] M. König, S. Wiedmann, C. Brüne, A. Roth, H. Buhmann, L. W. Molenkamp, X.-L. Qi and S.-C. Zhang, "Quantum Spin Hall Insulator State in HgTe Quantum Wells," *Science*, vol. 318, pp. 766-770, 2007.
- [24] R. J. Cava, H. Ji, M. K. Fuccillo, Q. D. Gibson and Y. S. Hor, "Crystal structure and chemistry of topological insulators," *Journal of Materials Chemistry C*, vol. 1, pp. 3176-3189, 2013.
- [25] L. I. Berger, "Properties of Semiconductors," in *Handbook of Chemistry and Physics*, 88 ed., D. R. Lide, Ed., Boca Raton, 2008.
- [26] C. R. Becker, C. Brüne, M. Schäfer, A. Roth, H. Buhmann and L. W. Molenkamp, "The influence of interfaces and the modulation doping technique on the magneto-transport properties of HgTe based quantum wells," *Physical Status Solidi C*, vol. 9, pp. 3382-3389, 2007.
- [27] L. M. Williams, P. Y. Lu and S. N. G. Chu, "Plasma-enhanced chemical vapor deposited HgTe-CdTe epitaxial superlattices," *Applied Physics Letters*, vol. 54, pp. 1329-1331, 1989.

- [28] W. L. Ahlgren, E. J. Smith, J. B. James, T. W. James, R. P. Ruth, E. A. Patten, R. D. Knox and J.-L. Staudenmann, "Photo-MOCVD growth of HgTe-CdTe superlattices," *Journal of Crystal Growth*, vol. 86, pp. 198-209, 1988.
- [29] T. L. Anderson, H. Krause and H. Brigitte, "Refinement of the Sb₂Te₃ and Sb₂Te₂Se structures and their relationship to nonstoichiometric Sb₂Te₃-ySe_y compounds," *Acta Crystallographica Section B*, vol. 30, pp. 1307-1310, 1974.
- [30] C. P. Vicente, J. L. Tirado, J. C. Adouby, A. A. Toure and G. Kra, "X-ray Diffraction and ¹¹⁹Sn Mossbauer Spectroscopy Study of a New Phase in the Bi₂Se₃-SnSe System: SnBi₄Se₇," *Inorganic chemistry*, vol. 38, pp. 2131-2135, 1999.
- [31] S. Nakajima, "The Crystal Structure of Bi₂Te₃-xSex," vol. 24, pp. 479-485, 1963.
- [32] R. W. G. Wyckoff, *Crystal Structures*, vol. 2, New York: J. Wiley and Sons, 1964.
- [33] Y. Xia, D. Qian, D. Hsieh, L. Wray, A. Pal, H. Lin, A. Bansil, D. Grauer, Y. S. Hor, R. J. Cava and M. Z. Hasan, "Observation of a large-gap topological-insulator class with a single Dirac cone on the surface," *Nature Physics*, vol. 5, pp. 398-402, 2009.
- [34] D. Hsieh, Y. Xia, D. Qian, L. Wray, F. Meier, J. H. Dil, J. Osterwalder, L. Patthey, A. V. Federov, H. Lin, A. Bansil, D. Grauer, Y. S. Hor, R. J. Cava and M. Z. Hasan, "Observation of Time-Reversal-Protected Single-Dirac-Cone Topological-Insulator States in Bi₂Te₃ and Sb₂Te₃," *Physical Review Letters*, vol. 103, p. 146401, 2009.
- [35] R. Sehr and L. R. Testardi, "The optical properties of p-type Bi₂Te₃/Sb₂Te₃ alloys between 2–15 microns," *Journal of Physics and Chemistry of Solids*, vol. 23, pp. 1219-1224, 1962.
- [36] Y. Ran, Y. Zhang and A. Vishwanath, "One-dimensional topologically protected modes in topological insulators with lattice dislocations," *Nature Physics*, vol. 5, pp. 298-303, 2009.
- [37] H. Zhang, C. X. Liu, X. L. Qi, X. Dai, Z. Fang and S. C. Zhang, "Topological insulators in Bi₂Se₃, Bi₂Te₃ and Sb₂Te₃ with a single Dirac cone on the surface," *Nature Physics*, vol. 5, pp. 438-742, 2009.
- [38] D. Hsieh, Y. Xia, D. Qian, L. Wray, J. H. Dil, F. Meier, J. Osterwalder, L. Patthey, J. G. Checkelsky, N. P. Ong, A. V. Federov, H. Lin, A. Bansil, D. Grauer, Y. S. Hor, R. J. Cava and M. Z. Hasan, "A tunable topological insulator in the spin helical Dirac transport regime," *Nature*, vol. 460, pp. 1101-1105, 2009.

- [39] Y. L. Chen, J. G. Analytis, J. H. Chu, Z. K. Liu, S. K. Mo, X. L. Qi, H. J. Zhang, D. H. Lu, X. Dai, Z. Fang, S. C. Zhang, I. R. Fisher, Z. Hussain and Z. X. Shen, "Experimental Realization of a Three-Dimensional Topological Insulator, Bi₂Te₃," *Science*, vol. 325, p. 178, 2009.
- [40] T. Arakane, T. Sato, S. Souma, K. Kosaka, K. Nakayama, M. Komatsu, T. Takahashi, Z. Ren, K. Segawa and Y. Ando, "Tunable Dirac cone in the topological insulator Bi_{2-x}Sb_xTe_{3-y}Se_y," *Nature Communications*, vol. 3, p. 636, 2012.
- [41] C. Z. Chang, J. Zhang, X. Feng, J. Shen, Z. Zhang, M. Guo, K. Li, Y. Ou, P. Wei, L. L. Wang, Z. Q. Ji, Y. Feng, S. Ji, X. Chen, J. Jia, X. Dai, Z. Fang, S. C. Zhang, K. He, Y. Wang, L. Lu, X. C. Ma and Q. K. Xue, "Experimental Observation of the Quantum Anomalous Hall Effect in a Magnetic Topological Insulator," *Science*, vol. 340, no. 6129, pp. 167-170, 2013.
- [42] A. Y. Kitaev, "Unpaired Majorana fermions in quantum wires," *Physics-Uspekhi*, vol. 44, pp. 131-136, 2001.
- [43] J. Wang, Q. Zhou, B. Lian and S. C. Zhang, "Chiral topological superconductor and half-integer conductance plateau from quantum anomalous Hall plateau transition," *Physical Review B*, vol. 92, p. 064520, 2015.
- [44] D. J. Leopold, M. L. Wroge and J. G. Broerman, "Optical properties of HgTe-CdTe superlattices," *Applied Physics Letters*, vol. 50, p. 924, 1987.
- [45] J. T. Cheung, "Epitaxial growth of Hg_{0.7}Cd_{0.3}Te by laser-assisted deposition," *Applied Physics Letters*, vol. 43, p. 255, 1998.
- [46] D. D. Edwall, E. R. Gertner and W. E. Tennant, "Liquid phase epitaxial growth of large area Hg_{1-x}Cd_xTe epitaxial layers," *Journal of Applied Physics*, vol. 55, p. 1453, 1983.
- [47] J. P. Faurie, A. Million and G. Jacquier, "Molecular beam epitaxy of CdTe and Cd_xHg_{1-x}Te," *Thin Solid Films*, vol. 90, pp. 107-112, 1982.
- [48] H. Wiedemeier and A. E. Uzpurvis, "Epitaxial Growth of Hg_{1-x}Cd_xTe by Chemical Vapor Transport," *Journal of the Electrochemical Society*, vol. 130, pp. 252-254, 1983.
- [49] S. K. Ghandhi and I. Bhat, "High quality Hg_{1-x}Cd_xTe epitaxial layers by the organometallic process," *Applied Physics Letters*, vol. 44, p. 779, 1984.
- [50] Y. Guldner, G. Bastard, J. P. Vieren, M. Voss, J. P. Faurie and A. Million, "Magneto-Optical Investigations of a Novel Superlattice: HgTe-CdTe," *Physical Review Letters*, vol. 51, p. 907, 1983.

- [51] S. Dvoretzky, N. Mikhailov, Y. Sidorov, V. Shvets, S. Danilov, B. Wittman and S. Ganichev, "Growth of HgTe Quantum Wells for IR to THz Detectors," *Journal of ELECTRONIC MATERIALS*, vol. 39, pp. 918-923, 2010.
- [52] J. Arias, M. Zandian, J. G. Pask, S. H. Shin, L. O. Bubulac, R. E. DeWames and W. E. Tennant, "Molecular-beam epitaxy growth and in situ arsenic doping of p-on-n HgCdTe heterojunctions," *Journal of Applied Physics*, vol. 69, p. 2143, 1991.
- [53] A. J. Noreika, R. F. C. Farrow, F. A. Shirland, W. J. Takei, J. Gregg Jr., S. Wood and W. J. Choyke, "Characterization of molecular beam epitaxially grown HgCdTe on CdTe and InSb buffer layers," *Journal of Vacuum Science & Technology A*, vol. 4, p. 2081, 1986.
- [54] R. Sporcken, M. D. Lange, S. Sivananthan and J. P. Faurie, "Molecular beam epitaxy and characterization of HgCdTe(111)B on Si(100)," *Applied Physics Letters*, vol. 59, p. 81, 1991.
- [55] P. Capper, Ed., *Properties of Narrow Gap Cadmium-based Compounds*, London: INSPEC, the Institution of Electrical Engineers, 1994.
- [56] C. R. Becker, V. Latussek, G. Landwehr and L. W. Molenkamp, "Inverted band structure of type-III HgTe / Hg_{1-x}Cd_xTe superlattices and its temperature dependence," *Physical Review B*, vol. 68, p. 035202, 2003.
- [57] M. A. Herman and M. Pessa, "Hg_{1-x}Cd_xTe-Hg_{1-y}Cd_yTe (0<x,y<1) heterostructures: Properties, epitaxy, and applications," *Journal of Applied Physics*, vol. 57, p. 2671, 1985.
- [58] C. J. Summers, E. L. Meeks and N. W. Cox, "Molecular beam epitaxial growth of CdTe, HgTe, and Hg_{1-x}Cd_xTe alloys," *Journal of Vacuum Science & Technology B*, vol. 2, p. 224, 1984.
- [59] J. B. Mullin and S. J. C. Irvine, "Vapour phase epitaxy of CdxHg_{1-x}Te organometallics," *Journal of Physics D*, vol. 14, p. L149, 1981.
- [60] P. Vohl and C. M. Wolfe, "Vapor phase growth of Hg_{1-x}Cd_xTe epitaxial layers," *Journal of Electronic Materials*, vol. 7, p. 659-678, 1978.
- [61] D. O. Scanlan, P. D. C. King, R. P. Singh, A. de la Torre, S. McKeown Walker, G. Balakrishnan, F. Baumberger and C. R. A. Catlow, "Controlling Bulk Conductivity in Topological Insulators: Key Role of Anti-Site Defects," *Advanced Materials*, vol. 24, p. 2154, 2012.
- [62] J. Zhang, Z. Peng, A. Soni, Y. Zhao, Y. Xiong, B. Peng, J. Wang, M. S. Dresselhaus and Q. Xiong, "Raman Spectroscopy of Few-Quintuple Layer Topological Insulator," *Nano Letters*, vol. 11, pp. 2407-2414, 2011.

- [63] B. Poudel, J. Yang, D. Z. Wang and Z. F. Ren, "High-Yield Synthesis of Single-Crystalline Antimony Telluride Hexagonal Nanoplates Using a Solvothermal Approach," *Journal of the American Chemical Society*, vol. 127, pp. 13792-13793, 2005.
- [64] D. Wang, D. Yu, M. Mo, X. Liu and Y. Qian, "Preparation and characterization of wire-like Sb₂Se₃ and flake-like Bi₂Se₃ nanocrystals," *Journal of Crystal Growth*, vol. 253, pp. 445-451, 2003.
- [65] H. Zhu, C. A. Richter, E. Zhao, J. E. Bonevich, W. A. Kimes, H.-J. Jang, H. Yuan, H. Li, A. Arab, O. Kirillov, J. E. Maslar, D. E. Ioannou and Q. Li, "Topological Insulator Bi₂Se₃ Nanowire," *Scientific Reports*, vol. 3, p. 1757, 2013.
- [66] D. Kong, J. C. Randel, H. Peng, J. J. Cha, S. Meister, K. Lai, Y. Chen, Z. X. Shen, H. C. Manoharan and Y. Cui, "Topological Insulator Nanowires and Nanoribbons," *Nano Letters*, vol. 10, pp. 329-333, 2010.
- [67] J. J. Cha, J. R. Williams, D. Kong, S. Meister, H. Peng, A. J. Bestwick, P. Gallagher, G. Goldhaber-Gordon and Y. Cui, "Magnetic Doping and Kondo Effect in Bi₂Se₃," *Nano Letters*, vol. 10, pp. 1076-1081, 2010.
- [68] H. M. Benia, C. Lin, K. Kern and C. R. Ast, "Reactive Chemical Doping of the Bi₂Se₃ Topological Insulator," *Physical Review Letters*, vol. 107, p. 177602, 2011.
- [69] J. G. Analytis, R. D. McDonald, S. C. Riggs, J. H. Chu, G. S. Boebinger and I. R. Fisher, "Two-dimensional surface state in the quantum limit of a topological insulator," *Nature*, vol. 461, pp. 960-964, 2010.
- [70] L. A. Wray, S.-Y. Xu, Y. Xia, Y. S. Hor, D. Qian, A. V. Federov, H. Lin, A. Bansil, R. J. Cava and M. Z. Hasan, "Observation of topological order in a superconducting doped topological insulator," *Nature Physics*, vol. 6, pp. 855-859, 2010.
- [71] Y. S. Hor, P. Roushan, H. Beidenkopf, J. Seo, D. Qu, J. G. Checkelsky, L. A. Wray, D. Hsieh, Y. Xia, S.-Y. Xu, D. Qian, M. Z. Hasan, N. P. Ong, A. Yazdani and R. J. Cava, "Development of ferromagnetism in the doped topological insulator," *Physical Review B*, vol. 81, p. 195203, 2010.
- [72] L. L. Chang, L. Esaki, W. E. Howard and R. Ludeke, "The Growth of a GaAs–GaAlAs Superlattice," *Journal of Vacuum Science and Technology*, vol. 10, p. 11, 1973.
- [73] A. Richardella, D. M. Zhang, J. S. Lee, A. Koser, D. W. Rench, A. L. Yeats, B. B. Buckley, D. D. Awschalom and N. Samarth, "Coherent heteroepitaxy of Bi₂Se₃ on GaAs (111)B," *Applied Physics Letters*, vol. 97, p. 262104, 2011.
- [74] X. Liu, D. J. Smith, J. Fan, Y. H. Zhang, H. Cao, Y. P. Chen, J. Leiner, B. J. Kirby, M. Dobrowolska and J. K. Furdyna, "Structural properties of Bi₂Te₃ and Bi₂Se₃ topological insulators grown by

- molecular beam epitaxy on GaAs(001) substrates," *Applied Physics Letters*, vol. 99, p. 171903, 2011.
- [75] Y. Y. Li, G. Wang, X. G. Zhu, M. H. Liu, C. Ye, X. Chen, Y. Y. Wang, K. He, L. L. Wang, X. C. Ma, H. J. Zhang, X. Dai, Z. Fang, X. C. Xie, Y. Liu, X. L. Qi, J. F. Jia, S. C. Zhang and Q. K. Xue, "Intrinsic Topological Insulator Bi₂Te₃ Thin Films on Si and Their Thickness Limit," *Advanced Materials*, vol. 22, pp. 4002-4007, 2010.
- [76] G. Zhang, H. Qin, J. Chen, X. He, L. Lu, Y. Li and K. Wu, "Growth of Topological Insulator Bi₂Se₃ Thin Films on SrTiO₃ with Large Tunability in Chemical Potential," *Advanced Functional Materials*, vol. 21, pp. 2351-2355, 2011.
- [77] S. Schreyeck, N. V. Tarakina, G. Karczewski, C. Schumacher, T. Borzenko, C. Brüne, H. Buhmann, C. Gould, K. Brunner and L. W. Molenkamp, "Molecular beam epitaxy of high structural quality Bi₂Se₃ on lattice matched InP(111) substrates," *Applied Physics Letters*, vol. 102, p. 041914, 2013.
- [78] M. Brahlek, N. Koirala, M. Salehi, N. Bansal and S. Oh, "Emergence of Decoupled Surface Transport Channels in Bulk Insulating," *Physical Review Letters*, vol. 113, p. 026801, 2014.
- [79] T. Ginley, Y. Wang and S. Law, "Topological insulator film growth by molecular beam epitaxy: a review," *Crystals*, vol. 6, p. 154, 2016.
- [80] T. Ginley and S. Law, "Growth of Bi₂Se₃ topological insulator films using a selenium cracker source," *Journal of Vacuum Science and Technology B*, vol. 34, p. 02L105, 2016.
- [81] X. Liu, D. J. Smith, J. Fan, Y. H. Zhang, H. Cao, Y. P. Chen, B. J. Kirby, N. Sun, S. T. Ruggiero, J. Leiner, R. E. Pimpinella, J. Hagmann, K. Tivakornsasithorn, M. Dobrowolska and J. K. Furdyna, "Topological Insulators Bi₂Se₃ and Bi₂Te₃ Grown by MBE on (001) GaAs Substrates," *AIP Conference Proceedings*, vol. 1416, pp. 105-108, 2011.
- [82] Y. Wang, T. Ginley and S. Law, "Growth of high-quality Bi₂Se₃ topological insulators using (Bi_{1-x}In_x)₂Se₃ buffer layers," *Journal of Vacuum Science and Technology B*, vol. 36, p. 02D101, 2018.
- [83] L. A. Walsh, A. J. Green, R. Addou, W. Nolting, C. R. Cormier, A. T. Barton, T. R. Mowli, R. Yue, N. Lu, J. Kim, M. J. Kim, V. P. LaBella, C. A. Ventrice, S. McDonnell, W. G. Vandenberghe, R. M. Wallace, A. Diebold and C. L. Hinkle, "Fermi Level Manipulation through Native Doping in the Topological Insulator Bi₂Se₃," *ACS Nano*, vol. 12, p. 6310–6318, 2018.
- [84] H. Hertz, "On the effect of ultraviolet light upon the electrical discharge," *Annalen der Physik*, vol. 31, p. 983, 1887.

- [85] A. Einstein, "On a Heuristic Viewpoint Concerning the Production and Transformation of Light," *Annalen der Physik*, vol. 17, p. 132, 1905.
- [86] S. Hüfner, *Photoelectron Spectroscopy*, vol. 75, Berlin: Springer, 1995, p. 473.
- [87] V. N. Strocov, R. Claessen, G. Nicolay, S. Hüfner, A. Kimura, A. Harasawa, S. Shin, A. Kakizaki, P. O. Nillson, H. I. Starnberg and P. Blaha, "Absolute band mapping by combined angle-dependent very-low-energy electron diffraction and photoemission: application to Cu," *Physical Review Letters*, vol. 81, p. 4943, 1998.
- [88] L. V. Yashina, E. V. Tikhonov, V. S. Neudachina, T. S. Zyubina, A. N. Chaika, V. I. Shtanov, S. P. Kobeleva and Y. A. Dobrovolsky, "The oxidation of PbTe(100) surface in dry oxygen," *Surface and Interface Analysis*, vol. 36, pp. 993-996, 2004.
- [89] J. Ihanus, E. Lambers, P. H. Holloway, M. Ritala and M. Leskelä, "XPS and electroluminescence studies on SrS_{1-x}Sex and ZnS_{1-x}Sex thin films deposited by atomic layer deposition technique," *Journal of Crystal Growth*, vol. 260, pp. 440-446, 2004.
- [90] V. V. Atuchin, V. A. Golyashov, K. A. Kokh, I. V. Korolkov, A. S. Kozhukhov, V. N. Kruchinin, S. V. Makarenko, L. D. Pokrovsky, I. P. Prosvirin, K. N. Romanyuk and O. E. Tereshchenko, "Formation of Inert Bi₂Se₃(0001) Cleaved Surface," *Crystal Growth and Design*, vol. 11, pp. 5507-5514, 2011.
- [91] J. A. Hagmann, X. Li, S. Chowdhury, S. N. Dong, S. Rouvimov, S. J. Pookpanratana, K. M. Yu, T. A. Orlova, T. B. Bolin, C. U. Segre, D. G. Seiler, C. A. Richter, X. Liu, M. Dobrowolska and J. K. Furdyna, "Molecular beam epitaxy growth and structure of self-assembled Bi₂Se₃/Bi₂MnSe₄ multilayer heterostructures," *New Journal of Physics*, vol. 19, p. 085002, 2017.
- [92] F. Meier, J. H. Dil, J. Lobo-Checa, L. Patthey and J. Osterwalder, "Quantitative vectorial spin analysis in angle-resolved photoemission: Bi/Ag(111) and Pb/Ag(111)," *Physical Review B*, vol. 77, p. 165431, 2008.
- [93] Y. H. Wang, D. Hsieh, D. Pilon, L. Fu, D. R. Gardner, Y. S. Lee and N. Gedik, "Observation of a Warped Helical Spin Texture in Bi₂Se₃ from Circular Dichroism Angle-Resolved Photoemission Spectroscopy," *Physical Review Letters*, vol. 107, p. 207602, 2011.
- [94] D. A. Long, *Raman Spectroscopy*, New York: MacGraw-Hill, 1977.
- [95] M. S. Dresselhaus, A. Jorio, M. Hofmann, G. Dresselhaus and R. Saito, "Perspectives on Carbon Nanotubes and Graphene Raman Spectroscopy," *Nano Letters*, vol. 10, pp. 751-758, 2010.
- [96] A. Das, S. Pisana, B. Chakraborty, S. Piscanec, S. K. Saha, U. V. Waghmare, K. S. Novoselov, H. R. Krishnamurthy, A. K. Geim, A. C. Ferrari and A. K. Sood, "Monitoring dopants by Raman scattering

- in an electrochemically top-gated graphene transistor," *Nature Nanotechnology*, vol. 3, pp. 210-215, 2008.
- [97] K. M. F. Shahil, M. Z. Hossain, V. Goyal and A. A. Balandin, "Micro-Raman spectroscopy of mechanically exfoliated few-quintuple layers of Bi₂Te₃, Bi₂Se₃, and Sb₂Te₃ materials," *Journal of Applied Physics*, vol. 111, p. 054305, 2012.
- [98] V. Gnezdilov, Y. G. Pashkevich, H. Berger, E. Pomjakushina, K. Conder and P. Lemmens, "Helical fluctuations in the Raman response of the topological insulator Bi₂Se₃," *Physical Review B*, vol. 84, p. 195118, 2011.
- [99] R. Valde's Aguilar, A. V. Stier, W. Liu, L. S. Bilbro, D. K. George, N. Bansal, L. Wu, J. Cerne, A. G. Makelz, S. Oh and N. P. Armitage, "Terahertz Response and Colossal Kerr Rotation from the Surface," *Physical Review Letters*, vol. 108, p. 087403, 2012.
- [100] W.-K. Tse and A. H. MacDonald, "Magneto-optical Faraday and Kerr effects in topological insulator films and in other layered quantized Hall systems," *Physical Review B*, vol. 84, p. 205327, 2011.
- [101] P. Di Pietro, M. Ortolani, O. Limaj, A. Di Gaspare, V. Giliberti, F. Giorgianni, M. Brahlek, N. Bansal, N. Koirala, S. Oh, P. Calvani and S. Lupi, "Observation of Dirac plasmons in a topological," *Nature Nanotechnology*, vol. 8, pp. 556-560, 2013.
- [102] Y. Wang, T. Ginley and S. Law, "Transport properties of Bi₂(Se_{1-x}Tex)₃ thin films grown by molecular beam epitaxy," *Journal of Vacuum Science and Technology B*, vol. 35, p. 02B106, 2017.
- [103] Z. Ren, A. A. Taskin, S. Sasaki, K. Segawa and Y. Ando, "Observations of two-dimensional quantum oscillations and ambipolar transport in the topological insulator Bi₂Se₃ achieved by Cd doping," *Physical Review B*, vol. 84, p. 075316, 2011.
- [104] K. Nomura, M. Koshino and S. Ryu, "Topological Delocalization of Two-Dimensional Massless Dirac Fermions," *Physical Review Letters*, vol. 99, p. 146806, 2007.
- [105] H. Suzuura and T. Ando, "Crossover from Symplectic to Orthogonal Class in a Two-Dimensional Honeycomb Lattice," *Physical Review Letters*, vol. 89, p. 266603, 2002.
- [106] J. Chen, H. J. Qin, J. Liu, T. Guan, F. M. Qu, G. H. Zhang, J. R. Shi, X. C. Xie, C. L. Yang, K. H. Wu, Y. Q. Li and L. Lu, "Gate-Voltage Control of Chemical Potential and Weak Antilocalization in Bi₂Se₃," *Physical Review Letters*, vol. 105, p. 176602, 2010.

- [107] J. G. Checkelsky, Y. S. Hor, R. J. Cava and N. P. Ong, "Bulk band gap and surface state conduction observed in voltage-tuned crystals of the topological insulator Bi₂Se₃," *Physical Review Letters*, vol. 106, p. 196801, 2011.
- [108] H.-T. He, G. Wang, T. Zhang, I.-K. Sou, G. K. L. Wong, J.-N. Wang, H.-Z. Lu, S.-Q. Shen and F.-C. Zhang, "Impurity Effect on Weak Antilocalization in the Topological Insulator Bi₂Te₃," *Physical Review Letters*, vol. 106, p. 166805, 2011.
- [109] L. Shubnikov and W. J. de Haas, "New phenomena in the change in resistance of bismuth crystals in a magnetic field at the temperature of liquid hydrogen," *Proceedings of the Royal Netherlands Academy of Arts and Science*, vol. 33, pp. 363-378, 418-432, 1930.
- [110] D. Shoenberg, *Magnetic Oscillations in Metals*, London: University Press, 1984.
- [111] J. G. Analytis, J.-H. Chu, Y. Chen, F. Corredor, R. D. McDonald, Z. X. Shen and I. R. Fisher, "Bulk Fermi surface coexistence with Dirac surface state in Bi₂Se₃: A comparison of photoemission and Shubnikov–de Haas measurements," *Physical Review B*, vol. 81, p. 205407, 2010.
- [112] D.-X. Qu, Y. S. Hor, J. Xiong, R. J. Cava and N. P. Ong, "Quantum Oscillations and Hall Anomaly of Surface States in the Topological Insulator Bi₂Te₃," *Science*, vol. 329, pp. 821-824, 2010.
- [113] Z. Ren, A. A. Taskin, S. Sasaki, K. Segawa and Y. Ando, "Large bulk resistivity and surface quantum oscillations in the topological insulator Bi₂Te₂Se," *Physical Review B*, vol. 82, p. 241306(R), 2010.
- [114] C. Brüne, A. Roth, H. Buhmann, E. M. Hankiewicz, L. W. Molenkamp, J. Maciejko, X.-L. Qi and S.-C. Zhang, "Spin polarization of the quantum spin Hall edge states," *Nature Physics*, vol. 8, pp. 485-490, 2012.
- [115] C. H. Li, O. M. J. van 't Erve, J. T. Robinson, Y. Liu, L. Li and B. T. Jonker, "Electrical detection of charge-current-induced spin polarization due to spin-momentum locking in Bi₂Se₃," *Nature Nanotechnology*, vol. 9, pp. 218-224, 2014.
- [116] C. H. Li, O. M. J. van 't Erve, S. Rajput, L. Li and B. T. Jonker, "Direct comparison of current-induced spin polarization in topological insulator Bi₂Se₃ and InAs Rashba states," *Nature Communications*, vol. 7, p. 13518, 2016.
- [117] V. M. Edelstein, "Spin polarization of conduction electrons induced by electric current in two-dimensional asymmetric electron systems," *Solid State Communications*, vol. 73, pp. 233-235, 1990.

- [118] A. Chernyshov, M. Overby, X. Liu, J. K. Furdyna, Y. Lyanda-Geller and L. P. Rokhinson, "Evidence for reversible control of magnetization in a ferromagnetic material by means of spin-orbit magnetic field," *Nature Physics*, vol. 5, pp. 656-659, 2009.
- [119] A. R. Mellnik, J. S. Lee, A. Richardella, J. L. Grab, P. J. Mintun, M. H. Fischer, A. Vaezi, A. Manchon, E. A. Kim, N. Samarth and D. C. Ralph, "Spin-transfer torque generated by a topological insulator," *Nature*, vol. 511, pp. 449-451, 2014.
- [120] Y. Wang, P. Deorani, K. Banerjee, N. Koirala, M. Brahlek, S. Oh and H. Yang, "Topological Surface States Originated Spin-Orbit Torques in Bi₂Se₃," *Physical Review Letters*, vol. 114, p. 257202, 2015.
- [121] C. X. Liu, X. L. Qi, X. Dai, Z. Fang and S. C. Zhang, "Quantum Anomalous Hall Effect in Hg_{1-y}MnyTe Quantum Wells," *Physical Review Letters*, vol. 101, p. 146802, 2008.
- [122] R. Yu, W. Zhang, H. J. Zhang, S. C. Zhang, X. Dai and Z. Fang, "Quantized Anomalous Hall Effect in Magnetic Topological Insulators," *Science*, vol. 329, pp. 62-64, 2010.
- [123] J. H. van Vleck, *The Theory of Electronic and Magnetic Susceptibilities*, London: Oxford University Press, 1932.
- [124] J. K. Furdyna, "Diluted magnetic semiconductors," *Journal of Applied Physics*, vol. 64, p. R29, 1988.
- [125] J. G. Checkelsky, R. Yoshimi, A. Tsukazaki, K. S. Takahashi, Y. Kozuka, J. Falson, M. Kawasaki and Y. Tokura, "Trajectory of the anomalous Hall effect towards the quantized state in a ferromagnetic topological insulator," *Nature Physics*, vol. 10, pp. 731-736, 2014.
- [126] C. Z. Chang, W. Zhao, D. Y. Kim, H. Zhang, B. A. Assaf, D. Heiman, S. C. Zhang, C. Liu, M. H. W. Chan and J. S. Moodera, "High-precision realization of robust quantum anomalous Hall state in a hard ferromagnetic topological insulator," *Nature Materials*, vol. 14, pp. 473-477, 2015.
- [127] A. P. Schnyder, S. Ryu, A. Furusaki and A. W. W. Ludwig, "Classification of topological insulators and superconductors in three spatial dimensions," *Physical Review B*, vol. 78, p. 195125, 2008.
- [128] L. Fu and C. Kane, "Superconducting Proximity Effect and Majorana Fermions at the Surface of a Topological Insulator," *Physical Review Letters*, vol. 100, pp. 1-4, 2008.
- [129] W. Dai, A. Richardella, R. Du, W. Zhou, X. Liu, C. X. Liu, S. H. Huang, R. Sankar, F. Chou, N. Samarth and Q. Li, "Proximity-effect-induced Superconducting Gap in Topological Surface States – A Point Contact Spectroscopy Study of NbSe₂/Bi₂Se₃ Superconductor-Topological Insulator Heterostructures," *Scientific Reports*, vol. 7, p. 7631, 2017.

- [130] M. X. Wang, C. Liu, J. P. Xu, F. Yang, L. Miao, M. Y. Yao, C. L. Gao, C. Shen, X. Ma, X. Chen, Z. A. Xu, Y. Liu, S. C. Zhang, D. Qian, J. F. Jia and Q. K. Xue, "The Coexistence of Superconductivity and Topological Order in the Bi₂Se₃ Thin Films," *Science*, vol. 336, pp. 52-55, 2012.
- [131] J.-P. Xu, M.-X. Wang, Z. L. Liu, J.-F. Ge, X. Yang, C. Liu, Z. A. Xu, D. Guan, C. L. Gao, D. Qian, Y. Liu, Q.-H. Wang, F.-C. Zhang, Q.-K. Xue and J.-F. Jia, "Experimental Detection of a Majorana Mode in the core of a Magnetic Vortex inside a Topological Insulator-Superconductor Bi₂Te₃/NbSe₂ Heterostructure," *Physical Review Letters*, vol. 114, p. 017001, 2015.
- [132] D. Zhang, J. Wang, A. M. DaSilva, J. S. Lee, H. R. Gutierrez, M. H. W. Chan, J. Jain and N. Samarth, "Superconducting proximity effect and possible evidence for Pearl vortices in a candidate topological insulator," *Physical Review B*, vol. 84, p. 165120, 2011.
- [133] J. A. Hagmann, X. Liu, M. Dobrowolska and J. K. Furdyna, "Investigation of anomalous magnetoresistance in topological insulator Bi₂Te₃ at the onset of superconductivity in indium contacts," *Journal of Applied Physics*, vol. 113, p. 17C724, 2013.
- [134] M. Kriener, K. Segawa, Z. Ren, S. Sasaki and Y. Ando, "Bulk Superconducting Phase with a Full Energy Gap in the Doped Topological Insulator CuxBi₂Se₃," *Physical Review Letters*, vol. 106, p. 127004, 2011.
- [135] B. D. Josephson, "Possible new effects in superconductive tunnelling," *Physics Letters*, vol. 1, pp. 251-253, 1962.
- [136] L. Fu and C. L. Kane, "Josephson current and noise at a superconductor/quantum-spin-Hall-insulator/superconductor junction," *Physical Review B*, vol. 79, p. 161408(R), 2009.
- [137] J. Wiedenmann, E. Bocquillon, R. S. Deacon, S. Hartinger, O. Herrmann, T. M. Klapwijk, L. Maier, C. Ames, C. Brüne, C. Gould, A. Oiwa, K. Ishibashi, S. Tarucha, H. Buhmann and L. W. Molenkamp, "4p-periodic Josephson supercurrent in HgTe-based topological Josephson junctions," *Nature Communications*, vol. 7, p. 10303, 2016.
- [138] K. Le Calvez, L. Veyrat, F. Gay, P. Plaidoux, C. B. Winkelmann, H. Courtois and B. Sacépé, "Joule overheating poisons the fractional ac Josephson effect in topological Josephson junctions," *Communications Physics*, vol. 2, p. 4, 2019.
- [139] E. Majorana, "A symmetric theory of electrons and positrons," *Nuovo Cimento*, vol. 14, p. 171, 1937.
- [140] C. Nayak, S. H. Simon, A. Stern, M. Freedman and S. Das Sarma, "Non-Abelian anyons and topological quantum computation," *Reviews of Modern Physics*, vol. 80, pp. 1083-1159, 2008.

- [141] J. D. Sau, S. Tewari, R. M. Lutchyn, T. D. Stanescu and S. Das Sarma, "Non-Abelian quantum order in spin-orbit-coupled semiconductors: Search for topological Majorana particles in solid-state systems," *Physical Review B*, vol. 82, p. 214509, 2010.
- [142] V. Mourik, k. Zuo, S. M. Frolov, S. R. Plissard, E. P. A. M. Bakkers and L. P. Kouwenhoven, "Signatures of Majorana Fermions in Hybrid Superconductor-Semiconductor Nanowire Devices," *Science*, vol. 336, pp. 1003-1007, 2012.
- [143] "Spin-resolved Andreev levels and parity crossings in hybrid superconductor–semiconductor nanostructures," *Nature Nanotechnology*, vol. 9, pp. 79-84, 2014.
- [144] E. Bocquillon, R. S. Deacon, J. Wiedenmann, P. Leubner, T. M. Klapwijk, C. Brüne, K. Ishibashi, H. Buhmann and L. W. Molenkamp, "Gapless Andreev bound states in the quantum spin Hall insulator HgTe," *Nature Nanotechnology*, vol. 12, pp. 137-143, 2017.
- [145] N. Read and D. Green, "Paired states of fermions in two dimensions with breaking of parity and time-reversal symmetries and the fractional quantum Hall effect," *Physical Review B*, vol. 61, p. 10267, 2000.
- [146] X.-L. Qi, T. L. Hughes and S.-C. Zhang, "Chiral topological superconductor from the quantum Hall state," *Physical Review B*, vol. 82, p. 184516, 2010.
- [147] J. Wang, Q. Zhou, B. Lian and S.-C. Zhang, "Chiral topological superconductor and half-integer conductance plateau from quantum anomalous Hall plateau transition," *Physical Review B*, vol. 92, p. 064520, 2015.
- [148] Q. L. He, L. Pan, A. L. Stern, E. C. Burks, X. Che, G. Yin, J. Wang, B. Lian, Q. Zhou, E. S. Choi, K. Murata, X. Kou, Z. Chen, T. Nie, Q. Shao, Y. Fan, S.-C. Zhang, K. Liu, J. Xia and K. L. Wang, "Chiral Majorana fermion modes in a quantum anomalous Hall insulator–superconductor structure," *Science*, vol. 357, pp. 294-299, 2017.
- [149] B. Lian, J. Wang, X.-Q. Sun, A. Vaezi and S.-C. Zhang, "Quantum phase transition of chiral Majorana fermions in the presence of disorder," *Physical Review B*, vol. 97, p. 125408, 2018.
- [150] R. Nitsche, H. U. Bölsterli and M. Lichtensteiger, "Crystal growth by chemical transport reactions—I: Binary, ternary, and mixed-crystal chalcogenides," *Journal of Physics and Chemistry of Solids*, vol. 21, pp. 199-205, 1961.
- [151] A. Olin, B. Nolang, E. G. Osadchii, L. O. Ohman and E. Rosen, "Bismuth Compounds," in *Chemical Thermodynamics of Selenium*, Amsterdam, Elsevier, 2005, pp. 196-203.

- [152] N. Levy, T. Zhang, J. Ha, F. Sharifi, A. A. Talin, Y. Kuk and J. A. Stroscio, "Experimental Evidence for s-Wave Pairing Symmetry in Superconducting $\text{CuxBi}_2\text{Se}_3$ Single Crystals Using a Scanning Tunneling Microscope," *Physical Review Letters*, vol. 110, p. 117001, 2013.
- [153] K. T. Law, P. A. Lee and T. K. Ng, "Majorana fermion induced resonant Andreev reflection," *Physical Review Letters*, vol. 103, p. 237001, 2009.
- [154] C. H. Li, O. M. J. van 't Erve, Y. Y. Li and B. T. Jonker, "Electrical Detection of the Helical Spin Texture in a p-type Topological Insulator Sb_2Te_3 ," *Scientific Reports*, vol. 6, p. 29533, 2016.